Cell Reports
Medicine

Article

Non-canonical inflammasome activation mediates the adjuvanticity of nanoparticles

Graphical abstract

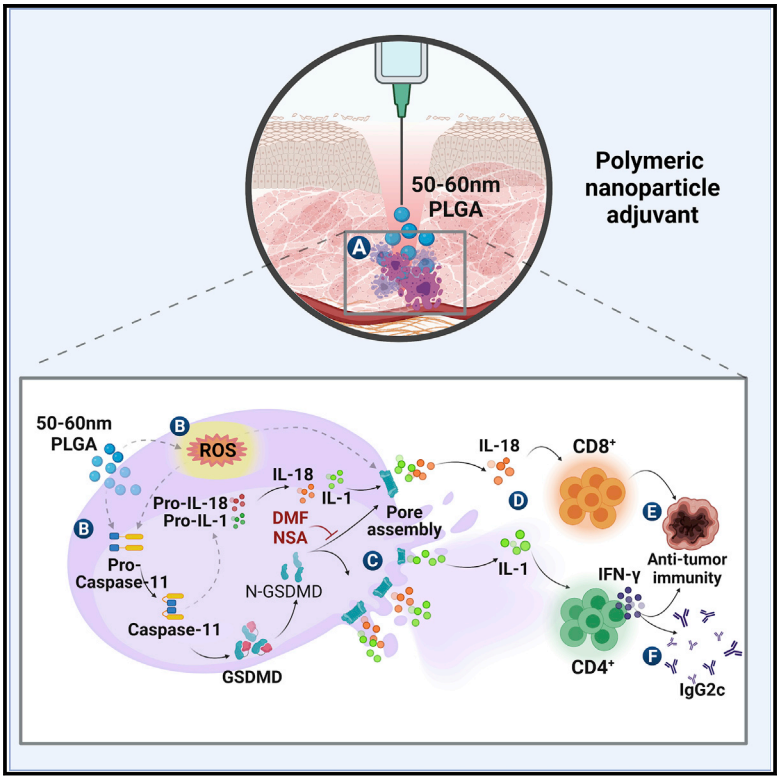

Highlights

- Adjuvant particle size dictates induction of Th1/CD8$^+$ responses but not antibodies
- 50- to 60-nm polymeric particles optimally induce cell-mediated (CMI) responses
- ROS, caspase-11, and gasdermin D are key mediators of nanoparticle-induced CMI
- Biodegradable 50- to 60-nm PLGA particles are promising CMI-inducing adjuvants

Authors

Natalia Muñoz-Wolf, Ross W. Ward, Claire H. Hearnden, ..., Yvonne Perrie, Emma Creagh, Ed C. Lavelle

Correspondence

lavellee@tcd.ie

In brief

Muñoz-Wolf et al. show that particle size dictates the induction of cell-mediated immunity by polymeric nanoparticulate adjuvants, identifying 50–60 nm as the optimal size for induction of Th1/CD8$^+$ responses. Authors provide mechanistic insights uncovering the roles of caspase-11, gasdermin D, and reactive oxygen species in nanoparticle adjuvant-induced cell-mediated immunity.

Muñoz-Wolf et al., 2023, Cell Reports Medicine *4*, 100899
January 17, 2023
https://doi.org/10.1016/j.xcrm.2022.100899

CellPress

Cell Reports Medicine

CellPress
OPEN ACCESS

Article

Non-canonical inflammasome activation mediates the adjuvanticity of nanoparticles

Natalia Muñoz-Wolf,[1,3,4,10] Ross W. Ward,[1,10] Claire H. Hearnden,[1] Fiona A. Sharp,[1] Joan Geoghegan,[6,7] Katie O'Grady,[1] Craig P. McEntee,[1] Katharine A. Shanahan,[9] Coralie Guy,[9] Andrew G. Bowie,[9] Matthew Campbell,[8] Carla.B. Roces,[5] Giulia Anderluzzi,[5] Cameron Webb,[5] Yvonne Perrie,[5] Emma Creagh,[9] and Ed C. Lavelle[1,2,11,*]

[1]Adjuvant Research Group, School of Biochemistry and Immunology, Trinity Biomedical Sciences Institute, Trinity College Dublin, Dublin 2 D02 R590, Ireland

[2]Centre for Research on Adaptive Nanostructures and Nanodevices (CRANN) & Advanced Materials Bio-Engineering Research Centre (AMBER), Trinity College Dublin, Dublin D02 PN40, Ireland

[3]Translational & Respiratory Immunology Lab, Department of Clinical Medicine, School of Medicine, Trinity Biomedical Sciences Institute, Dublin D02 R590, Ireland

[4]Clinical Medicine Tallaght University Hospital, Dublin D24 NR04, Ireland

[5]Strathclyde Institute of Pharmacy and Biomedical Sciences, University of Strathclyde, Glasgow G4 0RE, UK

[6]Department of Microbiology, Moyne Institute of Preventive Medicine, School of Genetics and Microbiology, Trinity College Dublin, Dublin, Ireland

[7]Institute of Microbiology and Infection, College of Medical and Dental Sciences, University of Birmingham, Birmingham B15 2TT, UK

[8]Smurfit Institute of Genetics, School of Genetics and Microbiology, Trinity College Dublin, Dublin, Ireland

[9]School of Biochemistry and Immunology, Trinity Biomedical Science Institute (TBSI), Trinity College Dublin, Dublin D02 R590, Ireland

[10]These authors contributed equally

[11]Lead contact

*Correspondence: lavellee@tcd.ie

https://doi.org/10.1016/j.xcrm.2022.100899

SUMMARY

The non-canonical inflammasome sensor caspase-11 and gasdermin D (GSDMD) drive inflammation and pyroptosis, a type of immunogenic cell death that favors cell-mediated immunity (CMI) in cancer, infection, and autoimmunity. Here we show that caspase-11 and GSDMD are required for $CD8^+$ and Th1 responses induced by nanoparticulate vaccine adjuvants. We demonstrate that nanoparticle-induced reactive oxygen species (ROS) are size dependent and essential for CMI, and we identify 50- to 60-nm nanoparticles as optimal inducers of ROS, GSDMD activation, and Th1 and $CD8^+$ responses. We reveal a division of labor for IL-1 and IL-18, where IL-1 supports Th1 and IL-18 promotes $CD8^+$ responses. Exploiting size as a key attribute, we demonstrate that biodegradable poly-lactic co-glycolic acid nanoparticles are potent CMI-inducing adjuvants. Our work implicates ROS and the non-canonical inflammasome in the mode of action of polymeric nanoparticulate adjuvants and establishes adjuvant size as a key design principle for vaccines against cancer and intracellular pathogens.

INTRODUCTION

Vaccination prevents an estimated 6 million deaths per year globally and allows enormous savings in medical care costs and infection-related disability.[1] Vaccine-induced protection has been mainly linked to potent and durable humoral immunity that can effectively control pathogens with a relatively stable antigen repertoire and associated toxins.[2] However, emerging viruses like SARS-CoV-2,[3] infections caused by other intracellular pathogens, and cancer[4] are more effectively controlled by $CD8^+$ cytotoxic T lymphocytes (CTL) and IFN-γ-producing T helper 1 (Th1) lymphocytes alone, or together with protective antibodies. Therefore, induction of CMI remains a critical frontier for modern vaccinology.

Subunit vaccines based on purified antigens require adjuvants to boost their immunogenicity and efficacy. However, while the particulate adjuvants in licensed subunit vaccines effectively promote antibody responses, they do not induce optimal cell-mediated immunity (CMI).[5] Several inorganic and polymeric nano- and microparticles have shown promise as CMI-inducing adjuvants in preclinical studies[6–11]; however, the use of formulations containing particles with dissimilar physicochemical attributes, modification of their surface chemistry, and the use of co-adjuvants have yielded contradictory results.[12] Our understanding of how physicochemical characteristics of particles (i.e., size, surface charge, topography, shape, etc.) influence the magnitude and type of adjuvant-induced immune responses and their mode of action (MOA) is therefore limited.[13] Identifying

the design principles that link particulate adjuvant characteristics to immune activation, particularly strong CMI, could transform particulate adjuvant design and accelerate vaccine development for intracellular pathogens and cancer.

Unlike pathogens, inorganic particulate vaccine adjuvants including alum and synthetic polymeric particles lack inherent ligands to engage pathogen recognition receptors such as Toll-like receptors (TLRs) that can activate antigen-presenting cells (APCs) to prime cognate naive T cells. Instead, their adjuvanticity is thought to rely on damage/danger-associated molecular patterns (DAMPs) and inflammatory cytokines released in response to cell stress or death. Cellular stress and immunogenic cell death lead to the release of IL-1 family cytokines that act as inducible DAMPs,[14] enhancing APC maturation, naive T cell priming, and T cell effector functions.[9,15–18] However, their roles in adjuvant-induced T cell responses are highly context dependent and not fully understood.[19]

Regulated immunogenic cell death (ICD) pathways, including pyroptosis and necroptosis, contribute to the release of the IL-1 family cytokines, IL-1α, IL-1β, and IL-18. Unlike necrosis, which typically leads to sudden DAMP release and transient inflammation, regulated ICD promotes the coordinated synthesis and activation of inducible DAMPs including pro-IL-1β and pro-IL-18, prior to cell death. This is crucial to provide the appropriate immunogenic environment for T cell activation.[20] While secretion of IL-1 and IL-18 has been traditionally linked to the activation of canonical caspase-1 inflammasomes, a non-canonical inflammasome using caspase-11 as a sensor has been also described.[20] Both canonical and non-canonical inflammasomes converge on the activation of pro-IL-1, pro-IL-18, and gasdermin D (GSDMD). GSDMD, the executor of pyroptosis, forms membrane pores facilitating release of IL-1, IL-18, and other leaderless proteins.[21] In addition, cellular stress leading to production of reactive oxygen species (ROS) has been linked to formation of the GSDMD pores and resultant pyroptosis.[22] Different types of cell death including necrosis,[23] apoptosis-like death,[24] and caspase-independent cytolysis[25] have been linked to adjuvant MOA. However, the role of regulated ICD downstream of non-canonical inflammasome activation has not been addressed for particulate adjuvants.

Using biocompatible polystyrene and biodegradable polylactic co-glycolic acid (PLGA) particles (50 nm–30 μm), we demonstrate that size critically determines the ability of particles to induce antigen-specific T CD8$^+$ and Th1 responses, without affecting their ability to induce antibodies. We unequivocally identify 50–60 nm as the optimal particle size range for eliciting specific Th1 and CD8$^+$ T cells to subunit protein antigens and show that vaccination with 50-nm particles induced a long-lasting and functional response that protected mice from B16-OVA melanoma. We show that the non-canonical inflammasome sensor caspase-11 and the pyroptosis effector GSDMD are essential components of nanoparticle-induced Th1 and CD8$^+$ T cell responses. We uncover a clear division of labor for the IL-1 family cytokines with IL-1 supporting Th1 and IL-18 promoting CD8$^+$ T cells responses. Finally, we show that polymeric nanoparticle-induced GSDMD activation and CMI after intramuscular vaccination are linked to ROS induction, which is a size-dependent phenomenon promoted by 50- to 60-nm particles.

RESULTS

Particle size critically determines adjuvant-induced CD8$^+$ T cell responses

Polymeric particulate adjuvants have exciting potential to enhance the effectiveness of subunit vaccines. While the ability of such adjuvants to enhance antibody responses is well established, their ability to promote CMI is ambiguous,[12] potentially as a result of a lack of consistency in the physicochemical properties of the particles tested. Size is the most basic particulate attribute that influences immunostimulatory properties,[12,26] but precisely how particle size influences the type and quality of adjuvant-induced immune responses remains unclear. For example, some reported micron-sized polymeric PLGA particles ($\sim$1 μm) as more effective enhancers of antibody responses than nanoparticles,[27] whereas others found similar antibody responses for PLGA particles between 110 and 900 nm in size.[28] Reports on induction of CTL and Th1 responses have also been contradictory, depending on the system used.[12,29–31]

Taking advantage of their monodisperse and biocompatible nature, we used endotoxin-free, negatively charged polystyrene (PS) particles ranging in size from 50 nm to 30 μm to establish the role of size in CMI induction in an intramuscular (i.m.) prime-boost regime with ovalbumin (OVA). Antigen (ag)-specific CD8$^+$ T cell responses were quantified by flow cytometry using H-2 Kb OVA SIINFEKL epitope tetramers (Figure S1A). Remarkably, only 50-nm particles significantly increased ag-specific CD8$^+$ T cells in spleens of vaccinated animals (Figures 1A–1C) and enhanced ag-specific secretion of IFN-γ in splenocytes (Figure 1D), which we previously demonstrated was CD4$^+$ T cell mediated.[9] In addition, 50-nm NPs outperformed both CpG 1826 and 2′3′cGAMP in eliciting antigen CD8$^+$ T cells (Figures S1B and S1C), and elevated class I tetramer$^+$ frequencies were also observed in magnetically sorted CD8$^+$ T cells (Figure S1E), suggesting that tetramer staining efficacy is dependent on sample composition. In contrast, all particles enhanced ag-specific IgG (Figure 1E), and this was comparable to responses following vaccination with antigen and CpG 1826 or 2′3′cGAMP (Figure S1D). Interestingly, ag-specific secretion of IL-10 was noted in splenocytes of animals vaccinated with 50-nm particles and restimulated with OVA (Figure S2A). This cytokine, although regulatory, has been found to enhance CD8$^+$ responses, anti-tumor immunity, and vaccine efficacy when present just after booster vaccination.[32] In contrast, IL-17 was not detected for any particle size (Figure S2B).

To further confirm that size was the main determinant of particle-induced CMI, we used the same formulations in an intraperitoneal (i.p.) vaccination protocol since vaccination route can impact factors regulating CD8$^+$ T cell cross-priming, including the kinetics of antigen and adjuvant transport and subsets of APC being targeted.[33,34] Only 50-nm particles elicited a robust ag-specific CD8$^+$ response via the i.p. route (Figures S3A and S3B), confirming the importance of size for CMI induction independent of vaccination route, whereas all particle sizes induced strong IgG responses (Figure S3C).

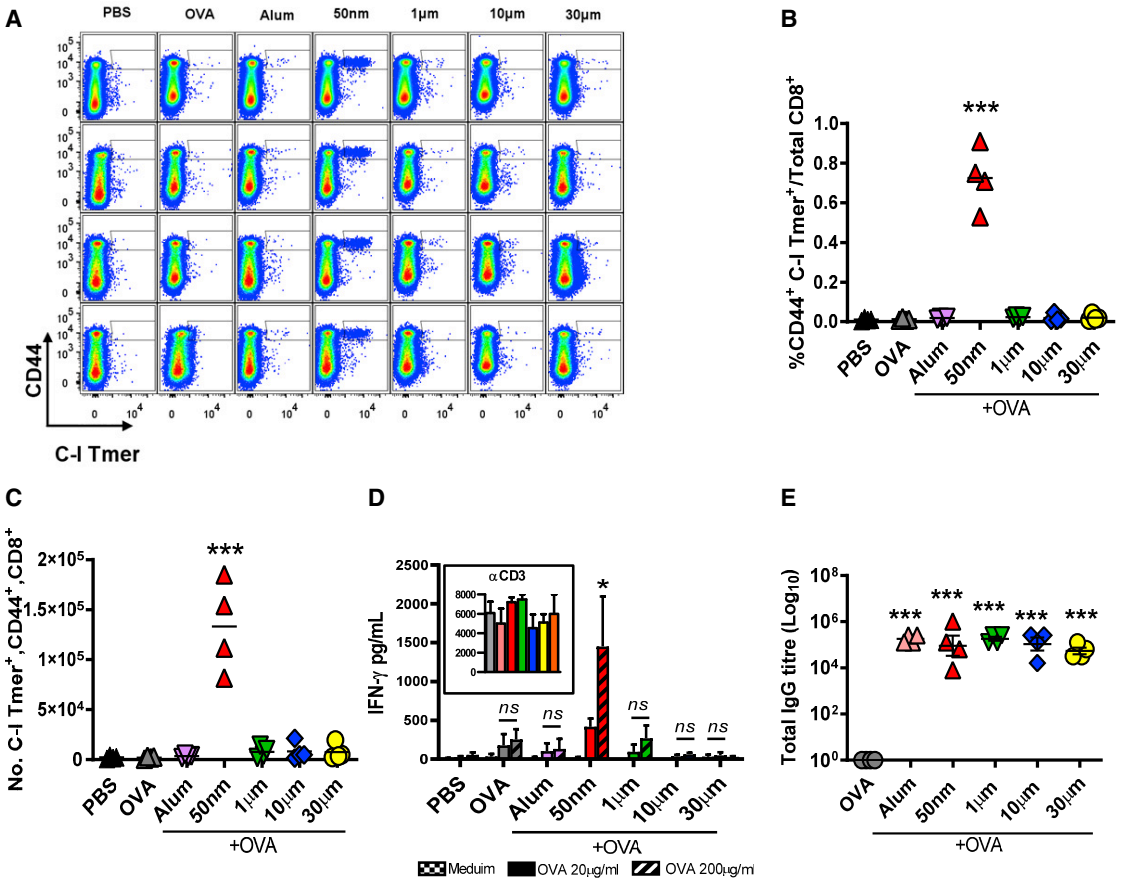

Figure 1. Particle size dictates the induction of T CD8$^+$ and IFN-γ responses

Effector CD8$^+$ T cells specific to the H-2 Kb OVA epitope SIINFEKL (C-I Tmer) were quantified tetramers 7 days after booster.

(A) Representative dot plots for SIINFEKL-specific CD8$^+$ and CD44$^+$.

(B and C) Percentage of CD44$^+$, Tmer$^+$ cells over total CD3$^+$, CD8$^+$, and total numbers in spleens.

(D) IFN-γ in splenocytes supernatants after *ex vivo* stimulation with OVA for 72 h.

(E) Total OVA-specific IgG titers in serum 7 days after booster. Statistical differences were calculated per multiple comparison ANOVA and Tukey-Kramer post-hoc test to determine significant differences between all groups on Log10 data. Representative of two experiments, n = 4/group.

Small nanoparticles elicit CD4$^+$ T cell responses and long-term memory after vaccination

CD4$^+$ T cell help during CD8$^+$ lymphocyte priming enhances CD8$^+$ memory and long-term protection.[35,36] Due to the poor performance of OVA I-A(b) tetramers, we took advantage of the influenza A nucleoprotein peptide QVYSLIRPNENPAHK ($NP_{311-325}$), a known class II restricted epitope in C57BL/6 mice, to evaluate the influence of particle size on ag-specific CD4$^+$ responses. Clinical grade alhydrogel (alum), an effective inducer of CD4$^+$ T cell responses,[37] was used as positive control. Particles in the 50-nm range were the only adjuvant to induce a potent ag-specific CD4$^+$ T cell response along with alum (Figure S4A).

To simultaneously evaluate CD8$^+$ and CD4$^+$ effector and memory T cell responses driven by 50-nm PS particles, we generated a fusion antigen by covalent linkage of $NP_{311-325}$ to the OVA protein (OVA–$NP_{311-325}$). The response was measured 7 days after i.m. booster. Co-administration of the fusion antigen with 50-nm particles significantly enhanced CD4$^+$ (Figure S4B) and CD8$^+$ T cell responses (Figure S4C) compared with the antigen alone. Importantly, ag-specific CD8$^+$ T cells remained significantly upregulated 100 days after immunization with admixed antigen and 50-nm particles, compared with mice vaccinated with OVA–$NP_{311-325}$ alone, and produced IFN-γ (Figure S4D). These long-lived CD8$^+$ T cells expressed the canonical memory marker CD69 and but no CD62L or CD103 (Figure S4D, histograms). Altogether these results reveal that size critically determines the ability of polymeric particles to promote ag-specific Th1 and CD8$^+$ T cell responses and identify 50 nm as the optimal size for induction of long-lasting CMI.

Polymeric 50-nm particles induce durable CD8$^+$ T cell-dependent responses against melanoma

To further assess the functionality of nanoparticle-induced CMI, we evaluated if vaccination with OVA and 50-nm particles conferred protection against B16-F10 melanoma cells expressing OVA (B16-OVA), where optimal protection requires

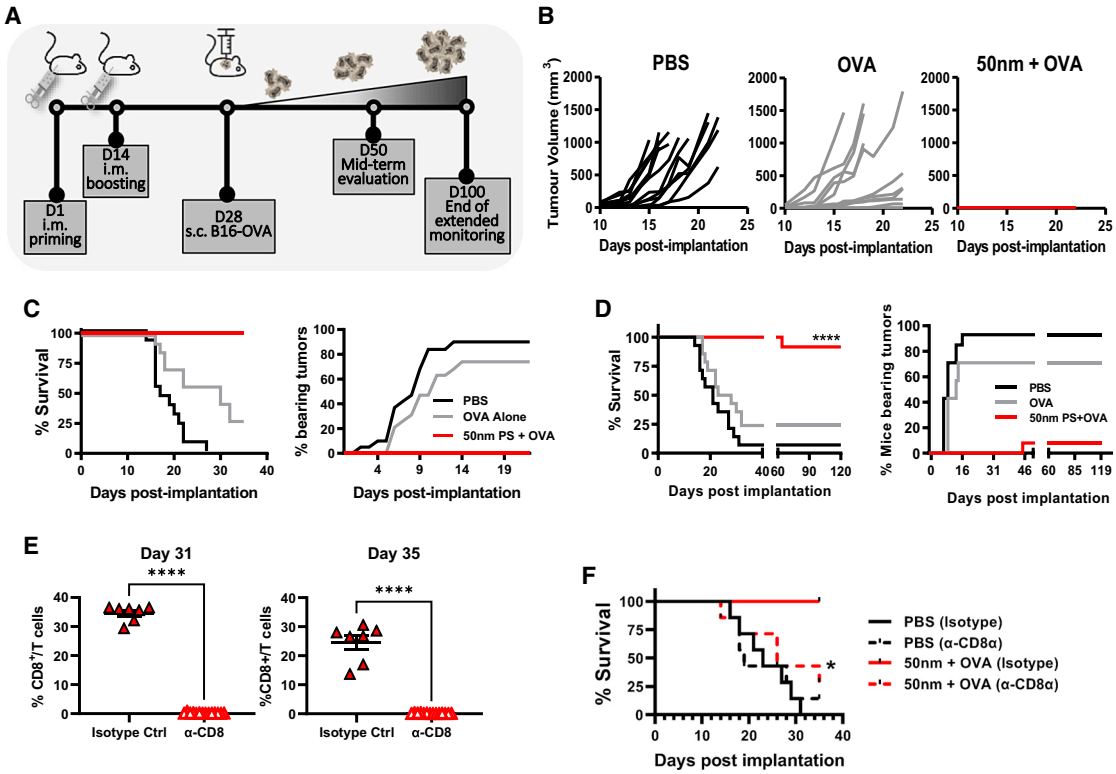

Figure 2. 50-nm PS nanoparticles drive potent antigen-specific anti-tumor immunity

(A) Immunization scheme and s.c. challenge with 3.5×10^5 B16-OVA cells. Tumors were measured daily.

(B) Spider plots show early development of tumors. Lines represent individual mice.

(C) Kaplan-Meier survival graphs up to 25 days after challenge.

(D) Extended survival analysis up to day 100. (A–C) n = 19 in PBS and OVA groups, n = 17 in 50-nm particle + OVA group. (D) n = 14 for PBS and OVA, n = 12 for 50-nm particle + OVA. Statistical significance for survival analyses determined by Mantel-Cox test.

(E) CD8α T cell depletion efficacy in peripheral blood by fluorescence-activated cell sorting over total $CD3^+$T cells on day 31 and 35 post priming displayed as mean frequency ± SEM. An unpaired T test was used to determine statistical significance where *p < 0.05, **p < 0.01, ***p < 0.001, and ****p < 0.0001.

(F) Kaplan-Meier survival analysis of challenged mice; a Mantel-Cox test was used to determine statistical significance between 50-nm NP OVA immunized mice with $CD8^+$T cell depletion and non-depleted 50-nm NP OVA immunized mice given isotype control where *p < 0.05. n = 7 mice per group.

IFN-γ, ag-specific $CD8^+$, and $CD4^+$ T cell responses. Mice were vaccinated i.m. with OVA alone or in combination with 50-nm particles. Fourteen days after booster, B16-OVA cells were implanted subcutaneously, and tumor growth was measured (Figure 2A). Mice vaccinated with 50-nm PS particles plus OVA were fully protected against melanoma, whereas all animals in the mock group (PBS) developed tumors and reached the endpoint by day 25 post-implantation. Vaccination with OVA alone delayed the development of tumors compared with PBS, but 80% of the animals still developed tumors within 2 weeks of implantation, and 75% succumbed to challenge by day 35 (Figures 2B and 2C). Extended monitoring for 100 days showed long-lasting protective immunity against melanoma in animals vaccinated with 50 nm + OVA (Figure 2D). To address whether the vaccine-induced CD8 responses were required for protection, $CD8^+$ T cells were depleted in vaccinated mice using an anti-CD8α targeted monoclonal antibody[38] (Figure 2E) leading to a reduction in vaccine-mediated protection from 100% to 30% (Figure 2F).

Size dictates the induction of CMI by biodegradable PLGA particles

To establish if size impacts the ability of particles made of a clinically relevant polymer to induce CMI, we used endotoxin-free PLGA (Tables S1 and S2). Owing to its safety, biodegradability, and biocompatibility, PLGA products including particles have been approved by the US Food and Drug Administration and the European Medicines Agency for parenteral, mucosal, subcutaneous, intradermal, and intramuscular drug delivery in humans.[39] While PLGA particle adjuvant properties were first described by O'Hagan et al. in the 1990s,[40] PLGA-based adjuvants have failed to show a clear advantage of PLGA particles (i.e., as a CMI-inducing adjuvant) compared with alum and other licensed adjuvants.[39]

Standardization of PLGA nanoparticle manufacturing by traditional methods such as double emulsion or solvent evaporation has been challenging, especially below 100-nm-diameter range, leading to formulations with high polydispersity indexes (PDI) that contain a mix of nano- and microparticles.[41] To overcome

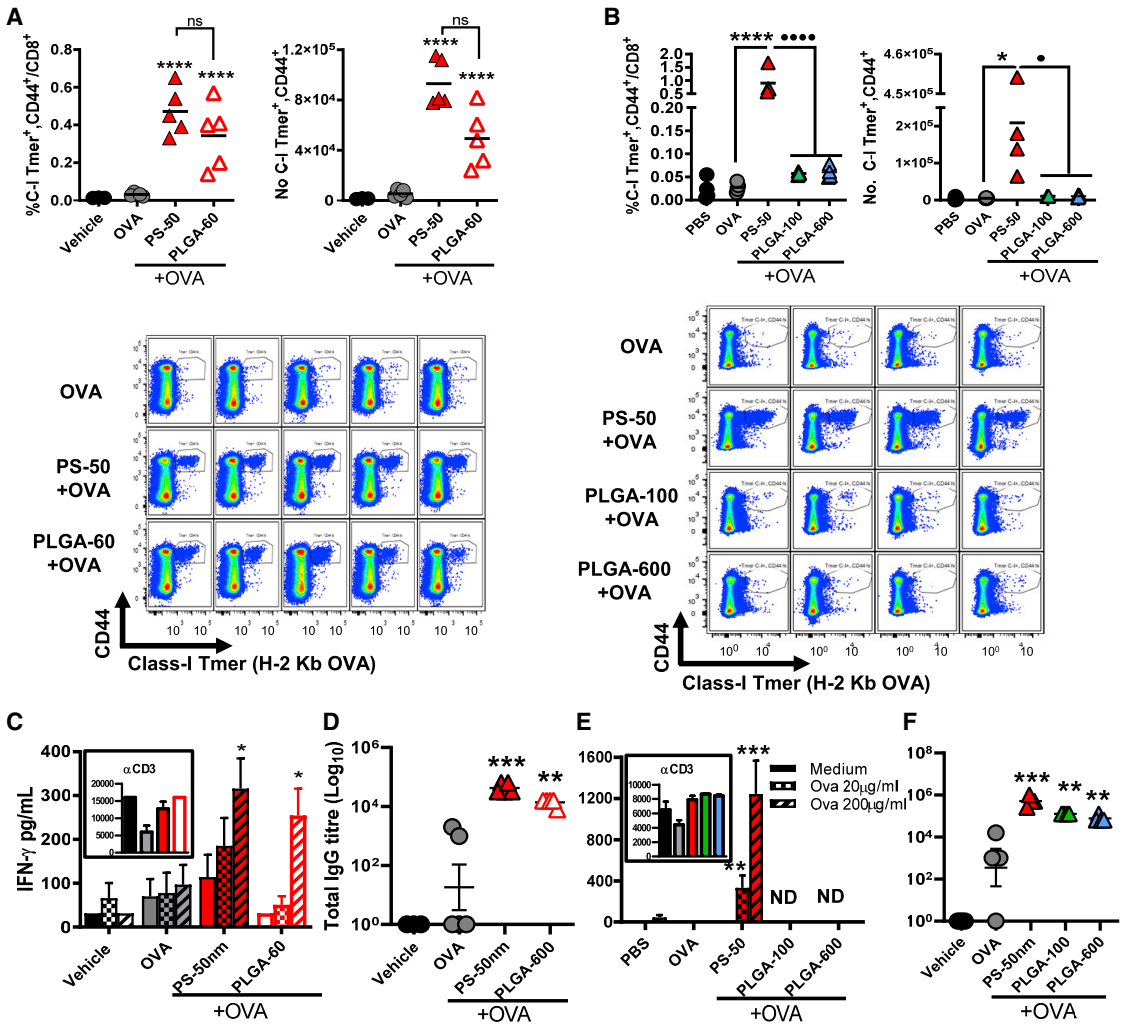

Figure 3. Induction of cell-mediated immunity by PLGA adjuvants depends on particle size

(A) An increase in percentage and total numbers of H-2Kb SIINFEKL-specific CD8$^+$ T cells is observed on day 21 after vaccination with 50-nm PS and 60-nm PLGA particles (graphs and dot plots).

(B) 100- and 500-nm PLGA particles fail to induce CD8$^+$ responses in the spleen after vaccination.

(C–E) IFN-γ in splenocytes supernatants after 72 h of ag-restimulation. Data are displayed as mean of triplicate samples ± SEM.

(D–F) OVA-specific IgG titers in serum 7 days after booster.

Statistical differences per multiple comparison ANOVA and Dunnett's or Fisher LSD post-hoc test. Representative of two experiments for (A), (C), and (D) and one for (B), (E), and (F). (A, C, D) n = 5 mice per group. (B, E, F) n = 4 mice per group. *p < 0.05, **p < 0.01, ***p < 0.001, and ****p < 0.0001; asterisks (*) represent differences to antigen alone, dots (•) represent comparisons between groups with adjuvant; ns: not significant.

this issue, we used the Nanoassemblr technology, a continuous-flow microfluidic platform designed for scale-up manufacturing of nanoparticles compliant with good manufacturing practice, and we produced PLGA nanoparticles of 61.6 ± 1.2 nm (PLGA-60) comparable to 53.7 ± 2.0 nm of the PS particles (PS-50), both with similar low PDIs and net negative charge (Table S1).

PLGA-60 and PS-50 were mixed with OVA and injected i.m. as before, both significantly enhancing ag-specific CD8$^+$ T cells compared with OVA alone (Figure 3A). PLGA-60 also induced IFN-γ secretion in ag-stimulated splenocytes (Figure 3C). In contrast, PLGA particles of 100 or 600 nm failed to induce CD8$^+$ T cell or Th1 responses when combined with OVA (Figures 3B and 3E). All particles induced significant ag-specific IgG independent of their size or polymer composition (Figures 3D and 3F). These results demonstrate that PLGA nanoparticulate adjuvants are potent inducers of CMI when formulated in the 50- to 60-nm size range.

Size-dependent induction of antigen-specific IFN-γ drives IgG2c class switching

T cell-derived cytokines influence antibody class switching. In rodents IFN-γ stimulates IgG2c/IgG2a in C57BL/6 or BALB/c mice respectively. Therefore, we investigated if the IFN-γ response induced by 50- to 60-nm particles influenced antibody isotypes induced by vaccination. As seen for total IgG titers

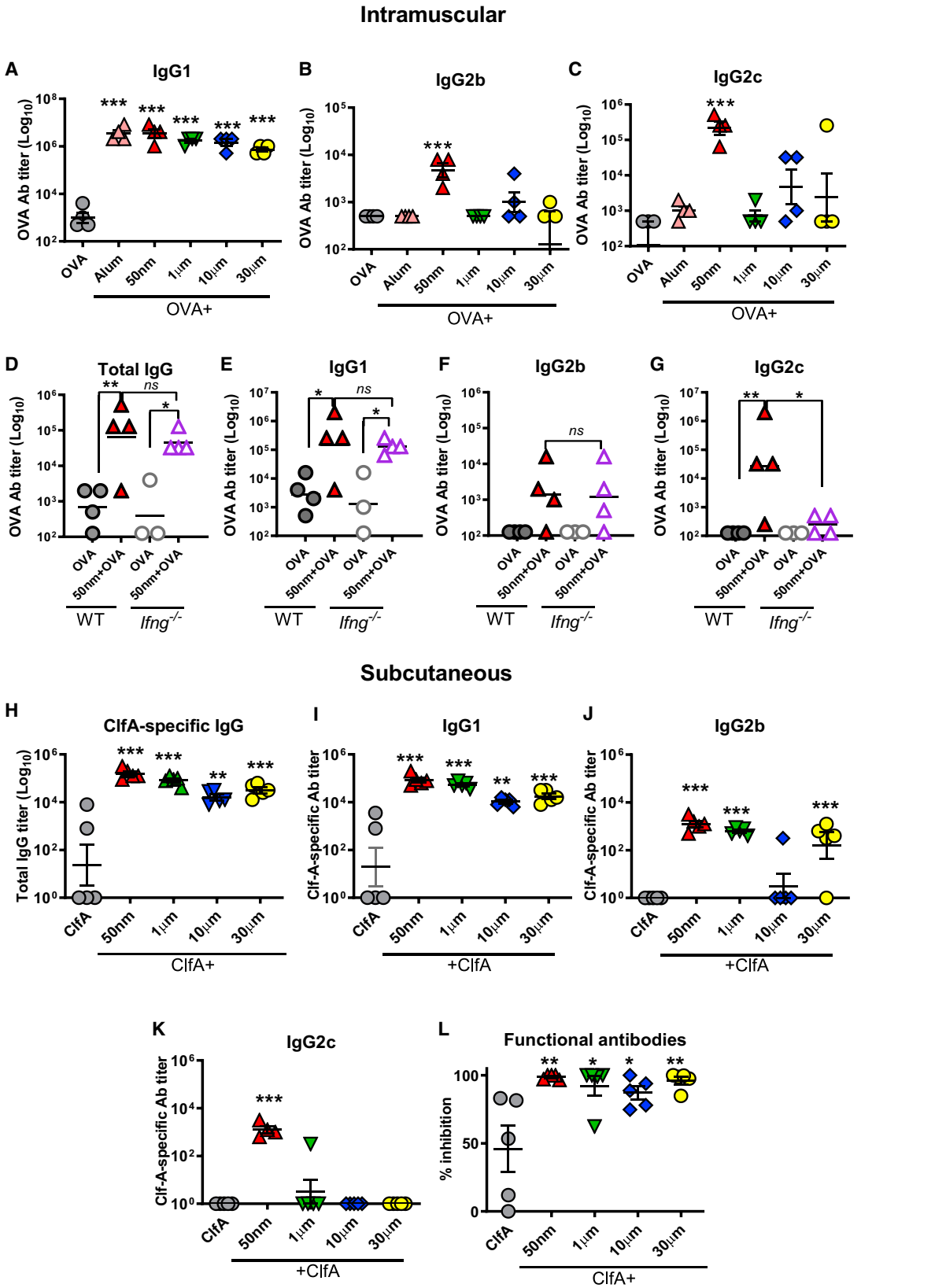

(legend on next page)

(Figures 1E, 3D, 3F, and S3C), particles across all sizes tested significantly enhanced OVA-specific IgG1 titers compared with OVA alone, similar to alum (Figure 4A). In contrast, only 50-nm particles significantly increased IgG2b and IgG2c titers (Figures 4B and 4C). To confirm whether class switching was IFN-γ dependent, we assessed antibodies *Ifng*$^{-/-}$ mice vaccinated with 50-nm PS + OVA. OVA-specific IgG, IgG1, and IgG2b were similar in *Ifng*$^{-/-}$ and WT mice (Figures 4D–4F), whereas IgG2c was negligible in *Ifng*$^{-/-}$ (Figure 4G). Interestingly, IFN-γ deficiency was associated with an increase in the number of ag-specific CD8$^+$ T cells (Figure S5).

To test if particle size influenced the functionality of antibodies, we measured humoral responses using a clinically relevant antigen: the staphylococcal clumping factor A (ClfA). This surface protein of *Staphylococcus aureus* binds to fibrinogen and fibrin, promoting bacterial adhesion to blood clots and is an important virulence factor during blood infection, septic arthritis, endocarditis, and skin infection.[42–45]

Mice were vaccinated subcutaneously (s.c.) with recombinant ClfA alone or in combination with particles, and serum antibodies were measured 7 days post-booster. All particles enhanced total ClfA-specific IgG and IgG1 titers (Figures 4H and 4I). However, only 50-nm particles were able to induce class switching to IgG2c (Figure 4K). Increased IgG2b titers were observed in animals vaccinated with 50-nm, 1-μm, and 30-μm particles (Figure 4J). This contrasts with the response seen with OVA for which only 50-nm particles were able to induce IgG2b and suggests that 50-nm particles are more appropriate adjuvants for poorly immunogenic antigens as they can induce a more diverse antibody response. Finally, we determined the capacity of the serum of vaccinated mice to inhibit *S. aureus* adhesion to immobilized fibrinogen *in vitro*. Importantly, despite the different isotype profiles observed, all particle sizes were able to induce antibodies with comparable neutralizing activity (Figure 4L).

IL-1 and IL-18 differentially regulate the IFN-γ and CD8$^+$ T cell responses induced by nanoparticles

Cytokines of the IL-1 family play central roles in the priming, expansion, and survival of T cells, either by promoting APC maturation or acting directly influencing lymphocytes.[19] IL1 and IL-18 have been implicated in the MOA of GLA-SE and saponin-containing adjuvants,[46,47] but other than the role of IL-33 as a negative regulator of polymeric particle-induced CMI previously described by our lab,[9] IL-1 family cytokines have not been shown to support nanoparticle adjuvant-induced CMI *in vivo*. Given the importance of IL-1 or IL-18 as CMI modulators, we investigated their role in Th1/CD8$^+$ responses induced by 50-nm particles and compared the response in WT, *Il1r1*$^{-/-}$, and *Il18*$^{-/-}$ mice after vaccination. Neither IL-1 nor IL-18 were required for IgG or IgG1 responses (Figures 5A and 5B). Surprisingly, IL-18 deficiency boosted IgG2b and IgG2c production, which remained unaffected by the lack of IL-1 signaling (Figures 5C and 5D).

On the other hand, IL-18 was required for ag-specific CD8$^+$ T cell responses induced by 50-nm particles: ag-specific CD8$^+$ T cell numbers were reduced in the spleens of *Il18*$^{-/-}$ mice compared with wild-type mice (Figures 5E and 5F). Although IL-1β can directly support the expansion and effector function of CD8$^+$ T cells,[15,16] there was no statistically significant decrease of OVA-specific CD8$^+$ T cells in *Il1r1*$^{-/-}$ mice compared with WT (Figures 5E and 5F). In contrast, nanoparticle-induced Th1 responses were impaired as revealed by the lower secretion of IFN-γ seen in splenocytes of vaccinated *Il1r1*$^{-/-}$ mice after *ex vivo* restimulation (Figure 5G). Intriguingly, vaccination of *Il18*$^{-/-}$ mice with nanoparticles consistently induced increased ag-specific IFN-γ secretion upon restimulation, which is in line with the increased IgG2c responses observed (Figure 5G). Antigen-specific IL-10 secretion was reduced in *Il1r1*$^{-/-}$ mice but unaffected in *Il18*$^{-/-}$ mice (Figure 5H). In sum, IL-1 and IL-18 support different aspects of CMI induced by 50-nm particles, with IL-18 playing a prominent role in the induction of ag-specific CD8$^+$ T cell responses, and IL-1 stimulating ag-specific IFN-γ and IL-10 secretion after vaccination with nanoparticles.

The non-canonical inflammasome sensor caspase-11 and the pyroptosis effector GSDMD are essential for nanoparticle-induced cell-mediated immunity

Infectious and non-infectious stimuli including pathogen associated molecular patterns (PAMPs), particulate matter, and other cellular stressors can trigger the assembly of inflammasomes and secretion of IL-1α, IL-1β, and IL-18. Both canonical caspase-1 and non-canonical caspase-11 inflammasomes promote secretion of these cytokines via direct or indirect activation mechanisms.[21] Therefore, we sought to determine if either of these inflammatory caspases could contribute to Ag-specific CMI induced by 50-nm polymeric nanoparticles.

Given that pyroptotic ICD is also a feature of inflammasome activation in certain contexts, we first tested whether 50-nm particles induced cell death *in vitro*. Quantification of cell death by lactate dehydrogenase (LDH) release assay in murine myotubes (the most abundant cell type exposed to the vaccine components during i.m. vaccination) after exposure to PS 50-nm particles showed a dose-dependent increase in cytotoxicity. In contrast, 1-μm particles did not induce LDH release. Importantly, the cytotoxic effect of 50-nm particles was moderate in

Figure 4. Particle size influences antibody class switching without affecting antibody neutralizing activity

Wild-type (WT) or *Ifng*$^{-/-}$ mice received i.m. OVA (A-G) or s.c. ClfA (H–L) alone or in combination with PS particles. PBS was used as vehicle control and alum as positive control. Serum antibodies were measured by ELISA on day 21.

(A–C) OVA-specific IgG1, IG2b, and IgG2b after i.m. vaccination.

(D–G) Total antibodies and isotypes in WT and *Ifng*$^{-/-}$.

(H) Total ClfA-specific antibodies after s.c. vaccination.

(I–K) ClfA-specific titers for IgG1, IG2b, and IgG2b after s.c. vaccination.

(L) Neutralizing activity as percent inhibition of *S. aureus* binding to fibrinogen, with 100% being bacterial adherence in the absence of serum.

Results are shown as mean ± SEM; symbols represent individual animals. Statistical differences were calculated per multiple comparison ANOVA and Dunnett's test compared with antigen alone or selected Fisher LSD for selected groups. Representative of two experiments for WT mice immunized with OVA (n = 4/group) or ClfA (n = 5/group) and one for *Ifng*$^{-/-}$ (n = 4/group).

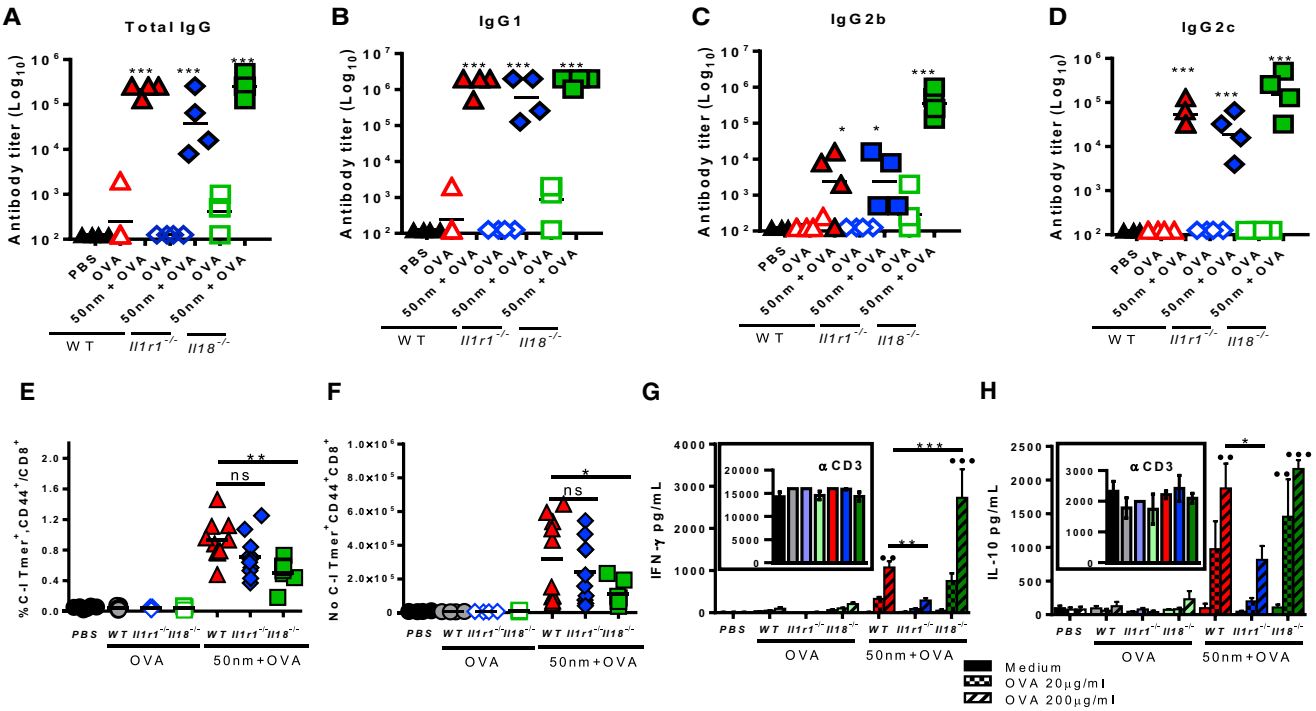

Figure 5. IL-1 and IL-18 differentially regulate nanoparticle-induced IFN-γ and CD8$^+$ T cell responses

(A–D) Ag-specific isotypes in serum 7 days after i.m. booster.

(E and F) Percentage and number of OVA H-2Kb CD8$^+$ T cells in spleens 7 days after booster.

(G and H) IFN-γ and IL-10 secretion in splenocytes on day 21, after 72h *ex vivo* ag-stimulation. Results are presented as mean ± SEM. Statistical differences are per one-way ANOVA and Fisher LSD (for Tmer$^+$ cell quantification) or Dunnett's (for cytokine quantification) post-hoc tests. IFN-γ and IL-10 data are shown as mean ± SEM; * denotes differences between selected groups, • denotes difference compared with control (OVA alone), ns: not significant. Representative of three experiments for *Il1r1*$^{-/-}$ mice and two for *Il18*$^{-/-}$ mice (n = 4/group for antibodies and 8/group for Tmer and cytokines).

comparison to other stimuli including alum, which typically induces necrotic cell death (Figure S6A), suggesting that 50-nm particles promote regulated ICD.

To assess the involvement of caspase-1 in 50-nm particle adjuvanticity, mice were vaccinated intramuscularly with 50-nm particles and OVA with or without the caspase-1 inhibitor Ac-YVAD-fmk (YVAD) during prime and boost. Pharmacological inhibition of caspase-1 did not significantly compromise induction of ag-specific CD8$^+$ T cells (Figures 6A and 6B), although a decrease in IFN-γ was noted (Figure 6C). YVAD did not affect antibody production induced by OVA + 50-nm particles (Figure S7A). In contrast, vaccination of caspase-11 knockout (*casp-11*$^{-/-}$) mice with 50-nm PS + OVA failed to promote ag-specific CD8$^+$ T cell (Figures 6D and 6E) and Th1 responses (4-fold decrease in IFN-γ) compared with wild-type mice (Figure 6F), while antibody responses remained intact in *casp11*$^{-/-}$ mice (Figure S7B).

Activation of caspase-11 leads to downstream cleavage of GSDMD oligomerization and transmembrane pores formation facilitating the release of IL-1β and IL-18 and pyroptotic cell death.[48–50] Therefore, we assessed whether polymeric particles could promote GSDMD cleavage in a size-dependent manner. Bone marrow-derived dendritic cells (BM-DCs) were primed with LPS and stimulated with 50-nm or 1-μm particles. Cell lysates were probed for cleaved GSDMD by western blot. As shown in Figure 6G, only 50-nm particles were able to induce GSDMD cleavage in BM-DCs.

To further define the contribution of GSDMD in particle-induced cell death, necrosulfonamide (NSA) and disulfiram (DMF) were used. NSA blocks pore formation by binding to the GSDMD Cys191 residue (murine Cys192) and blocking p30-GSDMD oligomerization. As a result, NSA selectively blocks pyroptosis and IL-1β release in human and murine cells without affecting TLR signaling, inflammasome assembly, or gasdermin E-mediated cell death.[51] It is important to note that while NSA has been reported to inhibit the necroptosis effector mixed lineage kinase domain-like (MLKL) protein, this is only observed in human cells.[52] DMF also blocks pyroptosis and cytokine release in murine and human cells by covalently modifying the Cys191/Cys192 residues of GSDMD and blocking pore formation.[53] Similar to our previous observation in myotubes (Figure S6A), 50-nm particles induced death in BM-DCs, which was prevented by the addition of the GSDMD inhibitors NSA and DMF (Figure S6B). These results suggest that 50-nm particles can promote pyroptotic cell death in immune and non-immune cells, favoring the release of active IL-1 and IL-18 to promote CD8$^+$ T cell activation and IFN-γ secretion.

Based on the *in vitro* data, we hypothesized that local cytotoxicity and release of IL-1 and IL-18 at the injection site through GSDMD pores were key to CMI. Therefore the GSDMD inhibitor

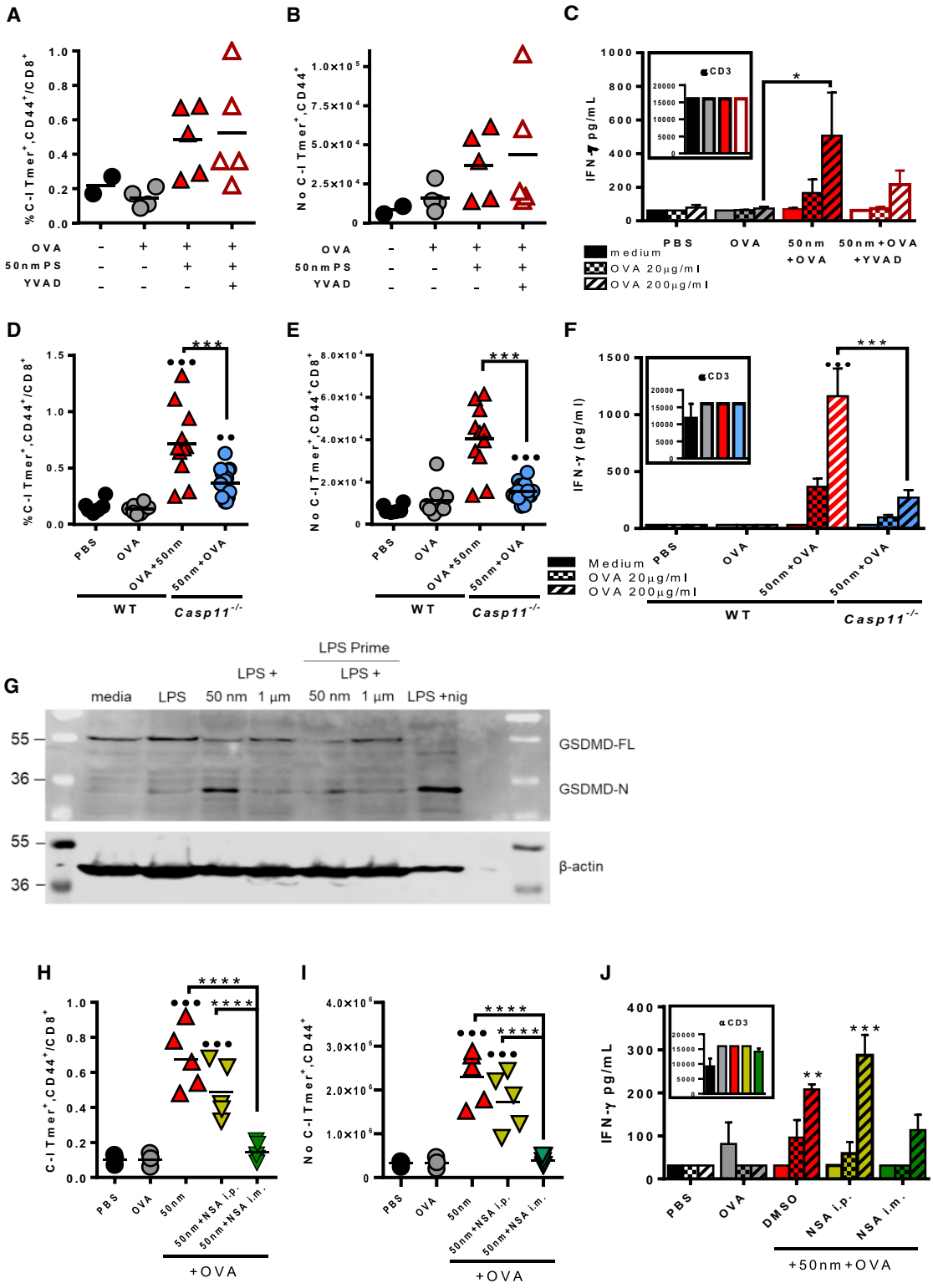

Figure 6. Caspase-11 and size-dependent induction of GSDMD are required for antigen-specific CD8⁺ responses

(A) WT mice were vaccinated i.m. with 50-nm particles and OVA, with or without the caspase-1 inhibitor Ac-YVAD-fmk (YVAD) on days 7 and 14. Ag-specific responses were quantified in splenocytes on day 21 using H-2Kb/OVA (SIINFEKL) MHC Tetramers. PBS or OVA alone were used as vehicle or antigen alone controls. Percentage of OVA-specific CD8⁺ over total CD8⁺ and CD44⁺ T cells.

(legend continued on next page)

NSA was administered *in vivo* either intraperitoneally 1 h prior to vaccination or locally in the muscle at the time of immunization. Systemic inhibition of GSDMD by i.p. injection of NSA induced a partial decrease in ag-specific $CD8^+$ T cells. In contrast, intramuscular NSA abolished ag-specific $CD8^+$ responses (Figures 6H and 6I), suggesting that local activation of GSDMD is necessary for CTL priming by 50-nm particles. Intramuscular administration of NSA at the time of vaccination also downregulated antigen-specific IFN-γ secretion, which was not affected in animals that received systemic NSA (Figure 6J). Inhibition of GSDMD had no impact on antibody responses regardless of the administration route (Figure S7C).

Polymeric nanoparticles promote size-dependent production of ROS which are required for induction of ag-specific $CD8^+$ responses after vaccination

ROS have been shown to influence the activity of both caspase-11 and GSDMD.[22,54] We therefore investigated if particles could induce cellular ROS in a size-dependent manner and if ROS production could contribute to particle adjuvanticity *in vivo*. Firstly, BM-DCs were stimulated with polymeric particles of 50 nm, 200 nm, or 1 μm diameter, and ROS production was measured by flow cytometry using Cell-ROX staining. Only 50-nm particles induced a notable increase in ROS production in viable cells (Figures 7A–7D), confirming that induction of cellular ROS by polymeric particles is a size-dependent phenomenon.

To assess whether ROS production was required for $CD8^+$ responses *in vivo*, mice were vaccinated i.m. with OVA and 50-nm particles and the ROS scavenger TEMPOL (4-hydroxy-2,2,6,6-tetramethyl piperidinoxyl), a membrane-permeable, metal-independent SOD mimetic specific for superoxide anions. Co-injection of OVA, 50-nm particles, and TEMPOL i.m. led to a significant reduction in the total number of ag-specific $CD8^+$ T cells in the spleen. In contrast, systemic i.p. administration of TEMPOL prior to and just after i.m. vaccination did not lead to decreased $CD8^+$ responses (Figure 7E).

These results indicate that local production of ROS elicited by 50-nm particles is essential for the induction of $CD8^+$ T cell responses.

DISCUSSION

Rational subunit vaccine development requires knowledge of how adjuvants activate and direct innate and adaptive immunity at a cellular and molecular level. Polymeric nano- and microparticles can enhance the immunogenicity of microbial and cancer antigens in preclinical vaccination models.[30,31,40,55] However, the design principles dictating their efficacy and the molecular mechanisms involved in their adjuvanticity are largely unknown, which has hindered their clinical development. Previously we showed that intramuscular vaccination with polymeric non-degradable biocompatible nanoparticles induced potent Th1 and $CD8^+$ T cell responses when combined with protein antigens.[9] Here we defined the key attributes of polymeric particle design linked to the induction of CMI, and we unveiled the molecular pathways required for their adjuvanticity.

Given the known role of programmed ICD in Th1 and $CD8^+$ T cell induction, we hypothesized that adjuvant-induced ICD could underlie activation of CMI by 50-nm particles. Supporting our hypothesis, 50-nm particles induced LDH release in skeletal muscle cells (Figure S6A), which was negligible for 1-μm particles. Likewise, 50-nm particles induced cell death in BM-DCs, which was prevented by the addition of the GSDMD inhibitors NSA and DMF (Figure S6B). In addition, stimulation of BM-DCs with polymeric particles induced a size-dependent activation of GSDMD that was only observed for 50-nm-particle-treated cells (Figure 6G). These results are suggestive of induction of pyroptotic cell death by 50-nm particles. In line with this, our *in vivo* data revealed a critical role for the non-canonical inflammasome sensor capase-11 (Figures 6D–6F), the pyroptosis effector GSDMD (Figures 6H–6J), and the pro-inflammatory cytokines IL-1 and IL-18 (Figures 5E–5G) in the induction of ag-specific CMI by 50-nm nanoparticles.

Enhanced ROS production has been shown to increase the expression and activation of caspase-11 downstream of c-Jun N-terminal kinase in a murine model of enteropathogenic bacterial infection,[54] and certain oxidized endogenous lipids have been identified as activator ligands for caspase-11.[56] Furthermore, ROS production influences the transition from GSDMD cleavage and membrane localization to oligomerization and pore formation.[22] Therefore, we hypothesized that 50-nm-particle-induced CMI dependent on caspase-11 and GSDMD activation could be linked to a size-dependent induction of ROS. Evidence for this size-dependency was provided by treating BM-DCs with 50-nm-, 200-nm-, and 1-μm-diameter particles and measuring ROS production by flow cytometry, which revealed that only 50-nm particles promoted significant ROS in these cells (Figures 7A–7D). Furthermore, intramuscular treatment of mice with the ROS scavenger TEMPOL at the time of vaccination abolished CMI, confirming the importance of locally generated ROS by 50-nm particles for induction of ag-specific $CD8^+$ T cells (Figure 7E).

(B) Total number of OVA-specific $CD8^+$ T cells in the spleen.
(C) Quantification of IFN-γ in culture supernatants 72 h after OVA stimulation.
(D and E) Analysis of H-2Kb/OVA (SIINFEKL) specific $CD8^+$ lymphocytes in vaccinated *Casp11*$^{-/-}$ and WT mice.
(F) Quantification of IFN-γ in culture supernatants 72 h after OVA stimulation.
(G) Induction of GSDMD is size dependent. BM-DCs were primed with LPS or left unprimed and were then stimulated with 50-nm or 1-μm particles in combination with LPS for 18 h. Cell lysates were probed for full-length and cleaved GSDMD protein, and β-actin was used as a loading control. LPS + Nigericin-treated BM-DCs were used as positive control for GSDMD cleavage. Data are representative of two independent experiments.
(H and J) WT mice were vaccinated as before. Some groups received the GSDMD inhibitor NSA i.p. 1 h before vaccination or i.m. at the time of vaccination. (G–H) Percentage and total number of OVA-specific $CD8^+$ T cells in the spleen.
(I) IFN-γ in culture supernatants 72 h after OVA stimulation. Statistical differences are per one-way ANOVA and Tukey-Kramer post-hoc test. Symbols: * denotes differences between treatment groups and • to OVA alone.
Representative for one experiment for (A)–(C) and (H)–(J) and two for (D)–(F) and (I). Each symbol represents one mouse.

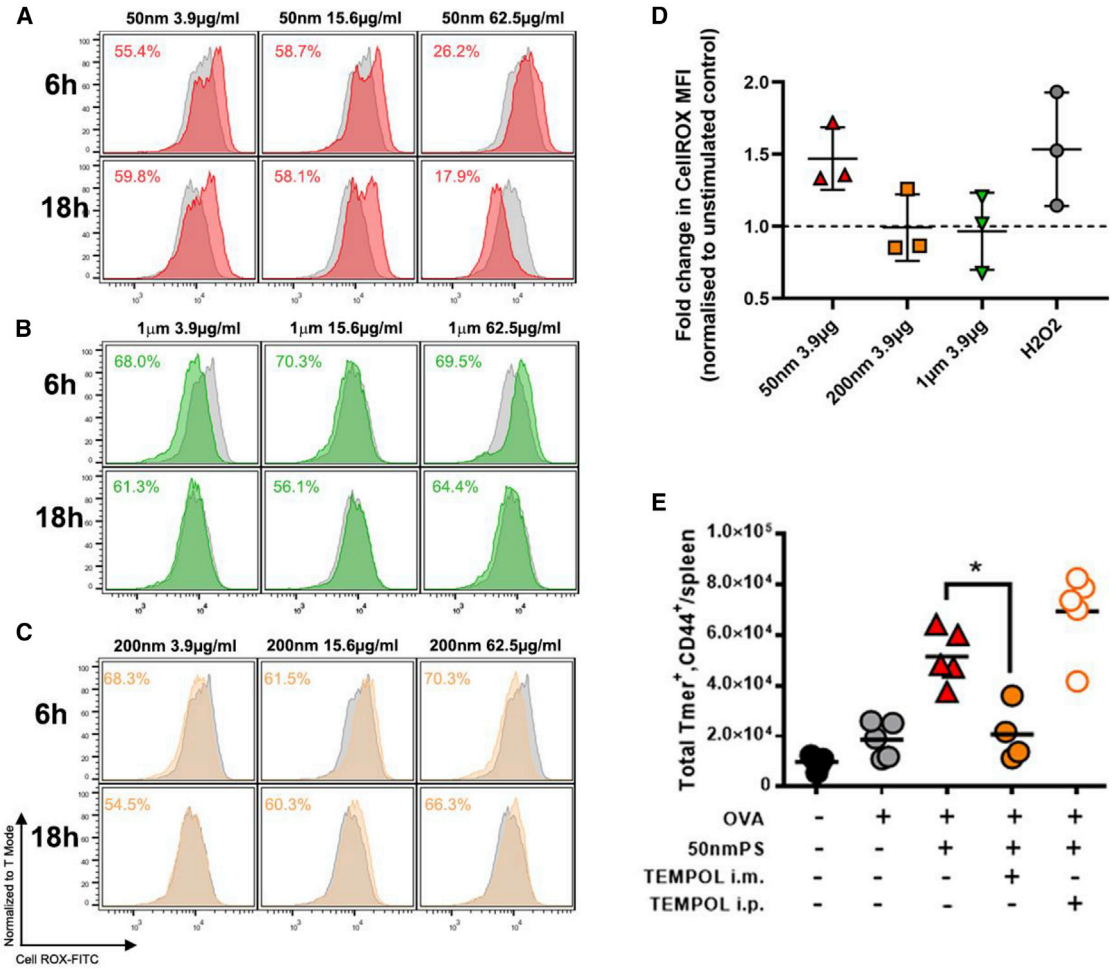

Figure 7. Size-dependent production of ROS controls the induction of CD8⁺ responses

(A–D) BM-DCs were stimulated with increasing concentrations of 50-nm (red), 200-nm (orange), or 1-µm (green) particles for 6 or 18 h or were left untreated (gray histograms). ROS production was measured by fluorescence-activated cell sorting on gated live cells using Cell-ROX gated on single live cells. Percentages in histograms indicate proportion of live cells after each treatment. (D) Mean fold change in Cell-ROX MFI compared with unstimulated bone marrow-derived dendritic cells controls is displayed ± SD. Data are representative of three biological/experimental repeats.

(E) Numbers of $CD44^{hi}$, $Tmer^{+}$, and $CD8^{+}$ T cells in spleens of WT mice treated with the ROS scavenger TEMPOL administered i.m. or i.p. during prime/boost. Statistical differences are per one-way ANOVA and Dunn's post-hoc test. Data are representative of one experiment. Each symbol represents one mouse.

Downstream of caspase-11 and GSDMD activation is the release of the pro-inflammatory cytokines IL-1 and IL-18 that can modulate $CD4^{+}$ and $CD8^{+}$ T cell responses.[9,15–19] IL-1 and IL-18 positively regulated nanoparticle-induced CMI, but we uncovered a clear division of labor for these inflammatory cytokines: while IL-1R1 signaling was required for optimal Th1 responses (Figure 5G), IL-18 supported ag-specific $CD8^{+}$ T cells (Figures 5E and 5F). Total IgG and IgG1 responses were comparable in *Il1r1*$^{-/-}$ and *Il18*$^{-/-}$ mice (Figures 5A and 5B), whereas IFN-γ production supported by IL-1R1 signaling was key to IgG2c class switching as revealed by *Ifng*$^{-/-}$ mice (Figures 5D and 5G). However, IFN-γ deficiency did not impair ag-specific $CD8^{+}$ T cell responses after vaccination (Figures S4A and S4B). Indeed, greater numbers of ag-specific $CD8^{+}$ T cells were seen in *Ifng*$^{-/-}$ mice. IFN-γ deficiency may lead to increased expansion of ag-specific $CD8^{+}$ T cells, possibly linked to altered immunodominance and reduced activation-induced cell death of $CD8^{+}$ lymphocytes.[57]

While IL-1R1 signaling and IFN-γ were dispensable for nanoparticle-induced $CD8^{+}$ T cell responses, IL-18 was required (Figures 5E and 5F). Intriguingly, we found an unexpected increase of IFN-γ production in *Il18*$^{-/-}$ mice after vaccination with 50-nm particles (Figure 5G). This is an interesting observation as IL-18 is known to promote Th1 function and IFN-γ production. Yet, IL-18 also supports the function of a specialized subset of regulatory T cells (Tregs) involved in tissue repair by promoting the expression of the growth factor amphiregulin (Areg) in damaged skeletal muscle.[58,59] Therefore, by impairing Areg expression on Tregs, IL-18 deficiency may lead to decreased Treg function and increased IFN-γ production.

Canonical (caspase-1) and non-canonical (caspase-11) inflammasomes lead to activation of IL-1α, IL-1β, and IL-18, and

secretion of these cytokines via formation of GSDMD pores, depending on the level of activation, may lead to pyroptotic cell death.[21] Although both caspase-1 and caspase-11 can process GSDMD into the active pore-forming subunits, caspase-1 but not caspase-11 can process IL-1β.[60] Both caspase-1 and caspase-11 (and its human ortholog capase-4) can process IL-18.[61] On the other hand, caspase-11 (and its human ortholog caspase-5) but not caspase-1 can process IL-1α,[62,63] which can also be processed by calpain activated via Ca^{2+} influx through the GSDMD pores. In fact, GSDMD deficiency impairs IL-1α maturation but does not affect IL-1β processing during inflammasome activation.[61] We found that local pharmacological inhibition of caspase-1 did not abrogate ag-specific cellular or humoral responses induced by 50-nm particles (Figures 6A–6C and S7A), whereas caspase-11 deficiency and GSDMD inhibition led to impaired Th1 and CD8 responses. This may point toward a role for IL-1α in promoting IL-1R1-dependent Th1 responses induced by the nanoparticulate adjuvant.

Finally, our study demonstrates that particle size critically determines the ability of particulate adjuvants to promote CMI and identifies 50–60 nm as the optimal range for induction of protective and long-lasting Th1 and $CD8^+$ T cell responses (Figures 1, 3, and S3). We also unveiled a dichotomy in terms of the particle qualities influencing the induction of humoral versus cellular responses: while only particles in the 50–60 nm range induced CMI, particles over a broad size range induced humoral responses of similar magnitude, irrespective of the polymer or immunization route (Figures 1E, 3F, 4H–4L, and S3C).

PLGA particles are attractive adjuvant candidates,[64] but to date, they have not demonstrated a unique selling point beyond widely used adjuvants including alum and oil in water emulsions. Our results suggest that the limited efficacy of PLGA particles as CMI-inducing adjuvants is linked to the use of inadequate particle sizes. We demonstrate that 50- to 60-nm PLGA nanoparticles effectively promote Th1 and $CD8^+$ T cell responses, which are abolished as soon as particle size reaches 100 nm (Figures 3A–3C). Until recently, limitations in PLGA particle formulation processes restricted their production to sizes between 80 nm and 250 μm. New nanoparticle manufacturing platforms such as the microfluidic technology used for preparation of our PLGA nanoparticles allow for fine control of particle size and generation of particles with low polydispersity index under GMP conditions that are appropriate for large-scale production.[65]

In summary, our study identifies size as a key design principle linking adjuvant particle characteristics to induction of $CD8^+$ and Th1 responses, demonstrates the efficacy of clinically relevant PLGA particles as CMI-inducing adjuvants, and implicates ROS production, the non-canonical inflammasome components caspase-11, GSDMD, and the effectors IL-1 and IL-18 as critical components of nanoparticulate adjuvant MOA. Our findings are a significant step forward toward the development of polymeric nanoparticles as next-generation adjuvants for anticancer and antiviral vaccines.

Limitations of the study

The current study is limited to a murine model of vaccination. Therefore, the magnitude of Th1 and $CD8^+$ responses elicited by polymeric nanoparticles in human subjects will require further investigation. Our results demonstrate the size-dependent nature of CMI and an optimal size range of 50–60 nm for the induction of $CD8^+$ T cell responses using polymeric nanoparticles, which differ in their composition, biodegradability profile, and charge. However, it remains to be determined if these findings apply to other particulate adjuvants including emulsions and liposomes. Finally, the *in vitro* studies mainly focused on analyzing the response of dendritic cells and myotubes, but further work is required to resolve the cell targets of adjuvant-induced ICD following injection locally and in the draining lymph nodes.

STAR★METHODS

Detailed methods are provided in the online version of this paper and include the following:

- KEY RESOURCES TABLE
- RESOURCE AVAILABILITY
  - Lead contact
  - Materials availability
  - Data and code availability
- EXPERIMENTAL MODEL AND SUBJECT DETAILS
  - Mice
  - Cell culture conditions
  - B16F10-OVA
  - Splenocytes
  - Culture of bone marrow derived dendritic cells (BMDCs)
  - Culture and differentiation of mouse myoblast cell line C2C12 cells
- METHOD DETAILS
  - Particle washing
  - PLGA particle synthesis
  - Antigen production
  - Mice immunisations
  - B16F-OVA melanoma challenge & CD8α T cell depletion
  - Quantification and characterization of ag-specific T cells
  - Quantification of cytokines
  - Quantification ag-specific antibodies
  - Magnetic sorting of $CD8^+$ T cells
  - Serum antibody neutralisation assay
  - Quantification of cell death
  - Immunoblotting
  - Cellular ROS quantification
  - Endotoxin quantification
- QUANTIFICATION AND STATISTICAL ANALYSIS

SUPPLEMENTAL INFORMATION

Supplemental information can be found online at https://doi.org/10.1016/j.xcrm.2022.100899.

ACKNOWLEDGMENTS

We thank Dr. Barry Moran, manager of the Flow Cytometry Facility and the Comparative Medicine Unit staff at Trinity Biomedical Sciences Institute for

their valuable assistance. We thank the NIH Tetramer Core Facility in the provision of tetramers. E.L., N.M.W., C.P.M., K.O., C.H.H., and R.W. received support from SFI investigator award 12/1A/1421 and Frontiers of the future award 19/FFP/6484. N.M.W. was also supported by the Irish Research Council (IRC) GOIPD-2017-1257, and Health Research Board (HRB) EIA-2019-004. R.W.W. received support from IRC GOIPG/2019/4236.

AUTHOR CONTRIBUTIONS

Conceptualization, E.C.L. and N.M.W. Methodology, N.M.W., R.W.W., Y.P., K.A.S., C.G., and A.G.B. Investigation N.M.W., R.W.W., C.P.M., K.O., C.H.H., F.A.S., C.B.C., G.A., J.G., K.A.S., C.G., and C.W. Writing – original draft, E.C.L. and N.M.W. Writing –review & editing, E.C.L., N.M.W., R.W.W., A.G.B., and E.C. Funding acquisition, E.C.L. Resources, E.C.L., Y.P., M.C., and E.C. Supervision, E.C.L., N.M.W., and A.G.B. Project management, E.C.L. Formal analysis and validation, N.M.W, C.H.H., and R.W.W. Visualization, N.M.W. and R.W.W.

DECLARATION OF INTERESTS

E.C.L. and N.M.W. are named inventors on patent application, WO2021123430, Polymeric nanoparticles as vaccine adjuvants. E.C.L. is a founder of AilseVax.

Received: January 31, 2022
Revised: July 24, 2022
Accepted: December 19, 2022
Published: January 17, 2023

REFERENCES

1. Bloom, D.E., Fan, V.Y., and Sevilla, J.P. (2018). The broad socioeconomic benefits of vaccination. Sci. Transl. Med. *10*, eaaj2345.
2. Rappuoli, R., and Aderem, A. (2011). A 2020 vision for vaccines against HIV, tuberculosis and malaria. Nature *473*, 463–469.
3. Cox, R.J., and Brokstad, K.A. (2020). Not just antibodies: B cells and T cells mediate immunity to COVID-19. Nat. Rev. Immunol. *20*, 581–582.
4. Gilbert, S.C. (2012). T-cell-inducing vaccines - what's the future. Immunology *135*, 19–26.
5. Pennock, N.D., Kedl, J.D., and Kedl, R.M. (2016). T cell vaccinology: beyond the reflection of infectious responses. Trends Immunol. *37*, 170–180.
6. Hamdy, S., Haddadi, A., Hung, R.W., and Lavasanifar, A. (2011). Targeting dendritic cells with nano-particulate PLGA cancer vaccine formulations. Adv. Drug Deliv. Rev. *63*, 943–955.
7. Kang, S., Ahn, S., Lee, J., Kim, J.Y., Choi, M., Gujrati, V., Kim, H., Kim, J., Shin, E.C., and Jon, S. (2017). Effects of gold nanoparticle-based vaccine size on lymph node delivery and cytotoxic T-lymphocyte responses. J. Contr. Release *256*, 56–67.
8. Neto, L.M.M., Zufelato, N., de Sousa-Júnior, A.A., Trentini, M.M., da Costa, A.C., Bakuzis, A.F., Kipnis, A., and Junqueira-Kipnis, A.P. (2018). Specific T cell induction using iron oxide based nanoparticles as subunit vaccine adjuvant. Hum. Vaccines Immunother. *14*, 2786–2801.
9. O'Grady, K., Hearnden, C.C.H., Bento, D., Oleszycka, E., Andersen, P., Muñoz-Wolf, N., and Lavelle, E.C. (2019). IL-33 is a negative regulator of vaccine-induced antigen-specific cellular immunity. J. Immunol. *202*, 1145–1152.
10. Zhang, Z., Tongchusak, S., Mizukami, Y., Kang, Y.J., Ioji, T., Touma, M., Reinhold, B., Keskin, D.B., Reinherz, E.L., and Sasada, T. (2011). Induction of anti-tumor cytotoxic T cell responses through PLGA-nanoparticle mediated antigen delivery. Biomaterials *32*, 3666–3678.
11. Zhou, W., Moguche, A.O., Chiu, D., Murali-Krishna, K., and Baneyx, F. (2014). Just-in-time vaccines: biomineralized calcium phosphate core-immunogen shell nanoparticles induce long-lasting CD8(+) T cell responses in mice. Nanomedicine *10*, 571–578.
12. Oyewumi, M.O., Kumar, A., and Cui, Z. (2010). Nano-microparticles as immune adjuvants: correlating particle sizes and the resultant immune responses. Expert Rev. Vaccines *9*, 1095–1107.
13. Lebre, F., Hearnden, C.H., and Lavelle, E.C. (2016). Modulation of immune responses by particulate materials. Adv. Mater. *28*, 5525–5541.
14. Martin, S.J. (2016). Cell death and inflammation: the case for IL-1 family cytokines as the canonical DAMPs of the immune system. FEBS J. *283*, 2599–2615.
15. Ben-Sasson, S.Z., Hogg, A., Hu-Li, J., Wingfield, P., Chen, X., Crank, M., Caucheteux, S., Ratner-Hurevich, M., Berzofsky, J.A., Nir-Paz, R., and Paul, W.E. (2013). IL-1 enhances expansion, effector function, tissue localization, and memory response of antigen-specific CD8 T cells. J. Exp. Med. *210*, 491–502.
16. Ben-Sasson, S.Z., Wang, K., Cohen, J., and Paul, W.E. (2013). IL-1beta strikingly enhances antigen-driven CD4 and CD8 T-cell responses. Cold Spring Harbor Symp. Quant. Biol. *78*, 117–124.
17. Schmitz, J., Owyang, A., Oldham, E., Song, Y., Murphy, E., McClanahan, T.K., Zurawski, G., Moshrefi, M., Qin, J., Li, X., et al. (2005). IL-33, an interleukin-1-like cytokine that signals via the IL-1 receptor-related protein ST2 and induces T helper type 2-associated cytokines. Immunity *23*, 479–490.
18. Vigne, S., Palmer, G., Lamacchia, C., Martin, P., Talabot-Ayer, D., Rodriguez, E., Ronchi, F., Sallusto, F., Dinh, H., Sims, J.E., and Gabay, C. (2011). IL-36R ligands are potent regulators of dendritic and T cells. Blood *118*, 5813–5823.
19. Munoz-Wolf, N., and Lavelle, E.C. (2018). A Guide to IL-1 family cytokines in adjuvanticity. FEBS J. *285*, 2377–2401.
20. Kayagaki, N., Warming, S., Lamkanfi, M., Vande Walle, L., Louie, S., Dong, J., Newton, K., Qu, Y., Liu, J., Heldens, S., et al. (2011). Non-canonical inflammasome activation targets caspase-11. Nature *479*, 117–121.
21. Abu Khweek, A., and Amer, A.O. (2020). Pyroptotic and non-pyroptotic effector functions of caspase-11. Immunol. Rev. *297*, 39–52.
22. Evavold, C.L., Hafner-Bratkovič, I., Devant, P., D'Andrea, J.M., Ngwa, E.M., Boršić, E., Doench, J.G., LaFleur, M.W., Sharpe, A.H., Thiagarajah, J.R., and Kagan, J.C. (2021). Control of gasdermin D oligomerization and pyroptosis by the Ragulator-Rag-mTORC1 pathway. Cell *184*, 4495–4511.e19. e4419.
23. Marichal, T., Ohata, K., Bedoret, D., Mesnil, C., Sabatel, C., Kobiyama, K., Lekeux, P., Coban, C., Akira, S., Ishii, K.J., et al. (2011). DNA released from dying host cells mediates aluminum adjuvant activity. Nat. Med. *17*, 996–1002.
24. Dupuis, M., Denis-Mize, K., LaBarbara, A., Peters, W., Charo, I.F., McDonald, D.M., and Ott, G. (2001). Immunization with the adjuvant MF59 induces macrophage trafficking and apoptosis. Eur. J. Immunol. *31*, 2910–2918.
25. Marty-Roix, R., Vladimer, G.I., Pouliot, K., Weng, D., Buglione-Corbett, R., West, K., MacMicking, J.D., Chee, J.D., Wang, S., Lu, S., and Lien, E. (2016). Identification of QS-21 as an inflammasome-activating molecular component of saponin adjuvants. J. Biol. Chem. *291*, 1123–1136.
26. Li, X., Sloat, B.R., Yanasarn, N., and Cui, Z. (2011). Relationship between the size of nanoparticles and their adjuvant activity: data from a study with an improved experimental design. Eur. J. Pharm. Biopharm. *78*, 107–116.
27. Gutierro, I., Hernández, R.M., Igartua, M., Gascón, A.R., and Pedraz, J.L. (2002). Size dependent immune response after subcutaneous, oral and intranasal administration of BSA loaded nanospheres. Vaccine *21*, 67–77.
28. Wendorf, J., Chesko, J., Kazzaz, J., Ugozzoli, M., Vajdy, M., O'Hagan, D., and Singh, M. (2008). A comparison of anionic nanoparticles and microparticles as vaccine delivery systems. Hum. Vaccine *4*, 44–49.
29. Nixon, D.F., Hioe, C., Chen, P.D., Bian, Z., Kuebler, P., Li, M.L., Qiu, H., Li, X.M., Singh, M., Richardson, J., et al. (1996). Synthetic peptides

entrapped in microparticles can elicit cytotoxic T cell activity. Vaccine *14*, 1523–1530.

30. Shen, H., Ackerman, A.L., Cody, V., Giodini, A., Hinson, E.R., Cresswell, P., Edelson, R.L., Saltzman, W.M., and Hanlon, D.J. (2006). Enhanced and prolonged cross-presentation following endosomal escape of exogenous antigens encapsulated in biodegradable nanoparticles. Immunology *117*, 78–88.
31. Allahyari, M., and Mohit, E. (2016). Peptide/protein vaccine delivery system based on PLGA particles. Hum. Vaccines Immunother. *12*, 806–828.
32. Fujii, S., Shimizu, K., Shimizu, T., and Lotze, M.T. (2001). Interleukin-10 promotes the maintenance of antitumor CD8+ T-cell effector function in situ. Blood *98*, 2143–2151.
33. Mohanan, D., Slütter, B., Henriksen-Lacey, M., Jiskoot, W., Bouwstra, J.A., Perrie, Y., Kündig, T.M., Gander, B., and Johansen, P. (2010). Administration routes affect the quality of immune responses: a cross-sectional evaluation of particulate antigen-delivery systems. J. Contr. Release *147*, 342–349.
34. Johansen, P., Mohanan, D., Martínez-Gómez, J.M., Kündig, T.M., and Gander, B. (2010). Lympho-geographical concepts in vaccine delivery. J. Contr. Release *148*, 56–62.
35. Cullen, J.G., McQuilten, H.A., Quinn, K.M., Olshansky, M., Russ, B.E., Morey, A., Wei, S., Prier, J.E., La Gruta, N.L., Doherty, P.C., and Turner, S.J. (2019). CD4(+) T help promotes influenza virus-specific CD8(+) T cell memory by limiting metabolic dysfunction. Proc. Natl. Acad. Sci. USA *116*, 4481–4488.
36. Zander, R., Schauder, D., Xin, G., Nguyen, C., Wu, X., Zajac, A., and Cui, W. (2019). CD4(+) T cell help is required for the formation of a cytolytic CD8(+) T cell subset that protects against chronic infection and cancer. Immunity *51*, 1028–1042.e4.
37. McKee, A.S., MacLeod, M., White, J., Crawford, F., Kappler, J.W., and Marrack, P. (2008). Gr1+IL-4-producing innate cells are induced in response to Th2 stimuli and suppress Th1-dependent antibody responses. Int. Immunol. *20*, 659–669.
38. Jung, S.R., Suprunenko, T., Ashhurst, T.M., King, N.J.C., and Hofer, M.J. (2018). Collateral damage: what effect does anti-CD4 and anti-CD8alpha antibody-mediated depletion have on leukocyte populations? J. Immunol. *201*, 2176–2186.
39. Danhier, F., Ansorena, E., Silva, J.M., Coco, R., Le Breton, A., and Préat, V. (2012). PLGA-based nanoparticles: an overview of biomedical applications. J. Contr. Release *161*, 505–522.
40. O'Hagan, D.T., Rahman, D., McGee, J.P., Jeffery, H., Davies, M.C., Williams, P., Davis, S.S., and Challacombe, S.J. (1991). Biodegradable microparticles as controlled release antigen delivery systems. Immunology *73*, 239–242.
41. Mohammadi-Samani, S., and Taghipour, B. (2015). PLGA micro and nanoparticles in delivery of peptides and proteins; problems and approaches. Pharmaceut. Dev. Technol. *20*, 385–393.
42. Josefsson, E., Hartford, O., O'Brien, L., Patti, J.M., and Foster, T. (2001). Protection against experimental Staphylococcus aureus arthritis by vaccination with clumping factor A, a novel virulence determinant. J. Infect. Dis. *184*, 1572–1580.
43. Kwiecinski, J., Jin, T., and Josefsson, E. (2014). Surface proteins of Staphylococcus aureus play an important role in experimental skin infection. APMIS *122*, 1240–1250.
44. McAdow, M., Kim, H.K., Dedent, A.C., Hendrickx, A.P.A., Schneewind, O., and Missiakas, D.M. (2011). Preventing Staphylococcus aureus sepsis through the inhibition of its agglutination in blood. PLoS Pathog. *7*, e1002307.
45. Moreillon, P., Entenza, J.M., Francioli, P., McDevitt, D., Foster, T.J., François, P., and Vaudaux, P. (1995). Role of Staphylococcus aureus coagulase and clumping factor in pathogenesis of experimental endocarditis. Infect. Immun. *63*, 4738–4743.
46. Desbien, A.L., Reed, S.J., Bailor, H.R., Dubois Cauwelaert, N., Laurance, J.D., Orr, M.T., Fox, C.B., Carter, D., Reed, S.G., and Duthie, M.S. (2015). Squalene emulsion potentiates the adjuvant activity of the TLR4 agonist, GLA, via inflammatory caspases, IL-18, and IFN-gamma. Eur. J. Immunol. *45*, 407–417.
47. Wilson, N.S., Duewell, P., Yang, B., Li, Y., Marsters, S., Koernig, S., Latz, E., Maraskovsky, E., Morelli, A.B., Schnurr, M., and Ashkenazi, A. (2014). Inflammasome-dependent and -independent IL-18 production mediates immunity to the iscomatrix adjuvant. J. Immunol. *192*, 3259–3268.
48. Kayagaki, N., Stowe, I.B., Lee, B.L., O'Rourke, K., Anderson, K., Warming, S., Cuellar, T., Haley, B., Roose-Girma, M., Phung, Q.T., et al. (2015). Caspase-11 cleaves gasdermin D for non-canonical inflammasome signalling. Nature *526*, 666–671.
49. Aglietti, R.A., Estevez, A., Gupta, A., Ramirez, M.G., Liu, P.S., Kayagaki, N., Ciferri, C., Dixit, V.M., and Dueber, E.C. (2016). GsdmD p30 elicited by caspase-11 during pyroptosis forms pores in membranes. Proc. Natl. Acad. Sci. USA *113*, 7858–7863.
50. Liu, X., Zhang, Z., Ruan, J., Pan, Y., Magupalli, V.G., Wu, H., and Lieberman, J. (2016). Inflammasome-activated gasdermin D causes pyroptosis by forming membrane pores. Nature *535*, 153–158.
51. Rathkey, J.K., Zhao, J., Liu, Z., Chen, Y., Yang, J., Kondolf, H.C., Benson, B.L., Chirieleison, S.M., Huang, A.Y., Dubyak, G.R., et al. (2018). Chemical disruption of the pyroptotic pore-forming protein gasdermin D inhibits inflammatory cell death and sepsis. Sci. Immunol. *3*, eaat2738.
52. Sun, L., Wang, H., Wang, Z., He, S., Chen, S., Liao, D., Wang, L., Yan, J., Liu, W., Lei, X., and Wang, X. (2012). Mixed lineage kinase domain-like protein mediates necrosis signaling downstream of RIP3 kinase. Cell *148*, 213–227.
53. Hu, J.J., Liu, X., Xia, S., Zhang, Z., Zhang, Y., Zhao, J., Ruan, J., Luo, X., Lou, X., Bai, Y., et al. (2020). FDA-approved disulfiram inhibits pyroptosis by blocking gasdermin D pore formation. Nat. Immunol. *21*, 736–745.
54. Lupfer, C.R., Anand, P.K., Liu, Z., Stokes, K.L., Vogel, P., Lamkanfi, M., and Kanneganti, T.-D. (2014). Reactive oxygen species regulate caspase-11 expression and activation of the non-canonical NLRP3 inflammasome during enteric pathogen infection. PLoS Pathog. *10*, e1004410.
55. Moon, J.J., Huang, B., and Irvine, D.J. (2012). Engineering nano- and microparticles to tune immunity. Adv. Mater. *24*, 3724–3746.
56. Zanoni, I., Tan, Y., Di Gioia, M., Broggi, A., Ruan, J., Shi, J., Donado, C.A., Shao, F., Wu, H., Springstead, J.R., and Kagan, J.C. (2016). An endogenous caspase-11 ligand elicits interleukin-1 release from living dendritic cells. Science *352*, 1232–1236.
57. Badovinac, V.P., Tvinnereim, A.R., and Harty, J.T. (2000). Regulation of antigen-specific CD8+ T cell homeostasis by perforin and interferon-gamma. Science *290*, 1354–1358.
58. Burzyn, D., Kuswanto, W., Kolodin, D., Shadrach, J.L., Cerletti, M., Jang, Y., Sefik, E., Tan, T.G., Wagers, A.J., Benoist, C., and Mathis, D. (2013). A special population of regulatory T cells potentiates muscle repair. Cell *155*, 1282–1295.
59. Zhang, C., Li, L., Feng, K., Fan, D., Xue, W., and Lu, J. (2017). Repair' Treg cells in tissue injury. Cell. Physiol. Biochem. *43*, 2155–2169.
60. Ramirez, M.L.G., Poreba, M., Snipas, S.J., Groborz, K., Drag, M., and Salvesen, G.S. (2018). Extensive peptide and natural protein substrate screens reveal that mouse caspase-11 has much narrower substrate specificity than caspase-1. J. Biol. Chem. *293*, 7058–7067.
61. Tsuchiya, K., Hosojima, S., Hara, H., Kushiyama, H., Mahib, M.R., Kinoshita, T., and Suda, T. (2021). Gasdermin D mediates the maturation and release of IL-1alpha downstream of inflammasomes. Cell Rep. *34*, 108887.
62. Gardner, S.E., Humphry, M., Bennett, M.R., and Clarke, M.C.H. (2015). Senescent vascular smooth muscle cells drive inflammation through an

interleukin-1alpha-dependent senescence-associated secretory phenotype. Arterioscler. Thromb. Vasc. Biol. *35*, 1963–1974.

63. Wiggins, K.A., Parry, A.J., Cassidy, L.D., Humphry, M., Webster, S.J., Goodall, J.C., Narita, M., and Clarke, M.C.H. (2019). IL-1alpha cleavage by inflammatory caspases of the noncanonical inflammasome controls the senescence-associated secretory phenotype. Aging Cell *18*, e12946.

64. Koerner, J., Horvath, D., and Groettrup, M. (2019). Harnessing dendritic cells for poly (D, L-lactide-co-glycolide) microspheres (PLGA MS)-Mediated anti-tumor therapy. Front. Immunol. *10*, 707.

65. Roces, C.B., Christensen, D., and Perrie, Y. (2020). Translating the fabrication of protein-loaded poly(lactic-co-glycolic acid) nanoparticles from bench to scale-independent production using microfluidics. Drug Deliv. Transl. Res. *10*, 582–593.

STAR★METHODS

KEY RESOURCES TABLE

REAGENT or RESOURCE	SOURCE	IDENTIFIER
Antibodies		
Anti-CD16/CD32 mAbs	BD Pharmingen	Cat# 553142; RRID: AB_394656
Anti-mouse F4/80 AF700 (Cl:A3-1)	Bio-Rad	Cat#: MCA497A700; RRID:AB_844537
Anti-mouse CD8 RPE-AF750(KT15)	Bio-Rad	Cat# MCA609P750; RRID:AB_616882
Anti-mouse CD4 APC-eFluor780 (GK1.5)	Invitrogen	Cat# 47-0041-82; RRID:AB_11218896
Anti-mouse CD3 BV650 (17A2)	Biolegend	Cat# 100229; RRID:AB_11204249
Anti-mouse CD11c BV605 (N418)	Biolegend	Cat# 563057; RRID:AB_2737978
Anti-mouse CD44 FITC (IM7)	BD Biosciences	Cat# 553133; RRID:AB_2076224
Anti-mouse B220 AF700 (RA3-6B2)	BD Biosciences	Cat# 557957; RRID:AB_396957
InVivoMab anti-mouse CD8α, Clone 2.43,	BE0061	Cat# BioXCell; RRID:AB_1125541
InVivoMab rat IgG2b isotype control, Clone LTF-2,	BE0090	Cat# BioXCell; RRID:AB_1107780
Biotinylated rat anti-mouse IgG1	BD Pharmingen	Cat# 553441; RRID:AB_394861
HRP conjugated goat anti-mouse IgG2c	AbD Serotec	Cat# STAR135P; RRID:AB_1102668
HRP conjugated Goat anti-mouse IgG	Southern Biotech	Cat# 1030-05; RRID:AB_2619742
Biotinylated rat anti-mouse IgG2b	BD Biosciences	Cat# 553393; RRID:AB_394831
Mouse anti-β-actin (AC-74) antibody	Sigma	Cat# A5316; RRID:AB_476743
Rabbit anti-GSDMD (126-138) antibody	Sigma	Cat# G7422; RRID:AB_1850381
IRDye 680RD Goat anti-mouse IgG Secondary AB	Licor	Cat# 926-68070; RRID:AB_10956588
IRDye 800CW Goat anti-Rabbit IgG Secondary AB	Licor	Cat# 926-32211; RRID:AB_621843
Bacterial and virus strains		
Staphylococcus aureus PS80	Laboratory of Joan Geoghegan	N/A
Chemicals, peptides, and recombinant proteins		
PE-labelled H-2K(b) Chicken OVA257-264 SIINFEKL	NIH	N/A
APC-labelled H-2K(b) I-A(b) NP311-325 QVYSLIRPNENPAHK	NIH	N/A
CellROX Green reagent	Invitrogen	C10444
Fixable Viability stain BV510	BD Biosciences	564406
Endograde Apyrogenic Ovalbumin	Lionex GmbH	LET0027
Necrosulfomide (NSA)	Millipore	480073
Dimethylfumarate (DMF)	Sigma	50744
Ac-YVAD-cmk	Cayman Chemical	10014
Influenza nucleoprotein peptide $NP_{311-325}$ (QVYSLIRPNENPAHK)	JPT Peptide Technologies	12489
Maleimide-activated OVA	Thermo-Fisher	77125
Recombinant *S. aureus* clumping factor A (ClfA)	Laboratory of Joan Geoghegan	N/A
Critical commercial assays		
IFN-γ DuoSet ELISA kit	R&D Systems	DY485
IL-17 DuoSet ELISA kit	R&D Systems	DY421
IL-10 ELISA MAX kit	Biolegend	431411
CyQUANT LDH Cytotoxicity Assay	Invitrogen	C20300

(*Continued on next page*)

Continued

REAGENT or RESOURCE	SOURCE	IDENTIFIER
Pierce Chromogenic Endotoxin Quantification Kit	Thermo Scientific	A39552
Experimental models: Cell lines		
B16F10-OVA	Laboratory of Kingston Mills, TCD	N/A
C2C12	ATCC	Cat# CRL-1772; RRID:CVCL_0188
Experimental models: Organisms/strains		
C57BL6/J	Comparative Medicines Unit, TCD	N/A
Il18$^{-/-}$	The Jackson Laboratory	Strain #:004130; RRID:IMSR_JAX:004130
Il1r1$^{-/-}$	The Jackson Laboratory	Strain #:003245; RRID:IMSR_JAX:003245
caspase11$^{-/-}$	Laboratory of Emma Creagh, TCD	N/A
Ifng$^{-/-}$	The Jackson Laboratory	Strain #:002287; RRID:IMSR_JAX:002287
Other		
Polystyrene particles (50nm–30μm)	Phosphorex Inc	50nm: 102; 1μm: 112; 10μm: 118; 30μm: 130
Alhydrogel (alum)	Brenntag Biosector/Croda	
Poly-lactic co-glycolic acid (PLGA) particles (>50nm size)	Phosphorex Inc	100nm: LG100; 500/600nm: LG500
50nm PLGA nanoparticles	Laboratory of Yvonne Perrie	N/A
Detoxi Gel	Thermo Fisher	20339

RESOURCE AVAILABILITY

Lead contact

Further information and requests for resources and reagents should be directed to and will be fulfilled by the lead contact, Ed Lavelle (lavellee@tcd.ie).

Materials availability

This study did not generate new unique reagents.

Data and code availability

- Data: All data reported in this paper will be shared by the lead contact upon request.
- Code: This paper does not report original code.
- Any additional information required to reanalyse the data reported in this paper is available from the lead contact upon request.

EXPERIMENTAL MODEL AND SUBJECT DETAILS

Mice

Eight to 12 weeks old wild-type (wt) C57BL/6J, *Il18*−/−, *Il1r1*−/−, *Casp11*−/−, *Ifng*−/− all on a C57BL/6 background were bred in-house in the Comparative Medicine Unit, TCD as per College and The Health Products Regulatory Authority (HPRA) welfare guidelines. All animal studies were approved by the TCD Animal Research Ethics Committee (Ethical Approval Number 091210) and HPRA license AE191364/P079. Animals were kept in IVC cages, SPF conditions with a 12h light cycle, 21°C, 50% relative humidity and food and water *ad libitum* for the duration of study. In selected experiments *Il18*−/−, *Il1r1*−/− and wt were maintained in the same conditions but in a low-barrier facility. Pilot studies were conducted to assess the response in males and females. No significant differences were found between sexes, therefore age- and sex-matched animals were used in all subsequent experiments. Power analyses were used to determine the minimal number of animals needed to achieve statistical significance according to 3Rs principles.

Cell culture conditions

All cells were cultured at 37°C with 95% humidity and 5% CO2, using a cell culture incubator. Base medium used for cell culture (RPMI 1640 (Gibco) or DMEM (SIGMA) was supplemented with 100 U/mL penicillin and 100μg/mL streptomycin (Gibco); 10% heat inactivated fetal bovine serum (FBS) (Biosera) and 2mM glutamine (Gibco) to make complete media (cRPMI or cDMEM). T cell media was made by supplementing RPMI 1640 0.04mM β-mercaptoethanol (Gibco), 0.88mM sodium pyruvate (Gibco),

0.88mM L-Glutamine (Gibco), 4.4 U/mL penicillin, 4.4μg/mL streptomycin (Gibco), 10mM MEM Non-Essential Amino Acid (Gibco), 0.35% (v/v) 100X MEM Vitamins (Gibco), 10% (v/v) heat-inactivated FBS (Biosera).

B16F10-OVA

B16F10 and B16F10-OVA cell lines were cultured in cDMEM and upon reaching logarithmic growth between 50-70% confluency were used for experimentation *in vivo*.

Splenocytes

Spleens were isolated from euthanised mice, and single cell suspensions were obtained after homogenizing the organs with a sterile plunger and filtering cell suspension in complete RPMI through 70μM cell strainers. Cells were centrifuged at 300 xg for 5 minutes at 4°C, and red blood cells (RBC) were lysed by suspending the cells in 1mL of 0.88% ammonium chloride (NH_4Cl) for 2 minutes, with subsequent quenching of reaction with cRPMI and centrifugation. Cells were resuspended in cRPMI and live cells counted with trypan blue. For *ex vivo* antigen restimulation assays, cells were plated in sterile U-bottom 96 well plates in 200μL of T cell media at 2×10^6 cells/mL. Cells were then restimulated with appropriate antigen concentrations and controls as detailed in the figure legends for each experiment.

Culture of bone marrow derived dendritic cells (BMDCs)

On day 1, the femurs and tibiae were removed from culled mice, and were cleaned of muscle tissue with a sterile scissors, tissue and 70% ethanol (EtOH). The separated bones were then briefly washed in petri dishes containing 70% EtOH and rinsed in cRPMI. A 20 mL syringe was filled with cRPMI and attached to a 27G needle. The tips of the femur and tibia bone were minimally cut using a sterile scissors and the bone marrow was flushed out into a petri dish utilising a 20mL syringe filled with cRPMI and a 27G needle. Cell clumps were disrupted by repeatedly passing the cell suspension through a 19G needle. The cells were transferred to 50 mL falcon tubes and centrifuged at 300 × g for 5 minutes at room temperature. The supernatant was removed, and the cell pellet was resuspended in 1 mL of 0.88% NH_4Cl de (NH_4Cl) for RBC for 2 minutes, with subsequent quenching of reaction with cRPMI and repeat of centrifugation. Supernatants were discarded and the cell pellet was resuspended in 10 mL cRPMI. Cells were counted as outline above and cell suspension volume was adjusted with cRPMI containing 20 ng/mL GM-CSF to give a final concentration of 4.25×10^5 cells/mL. Cells were transferred to T175 flasks (12.75×10^6 cells/flask) gently handling to avoid DC activation. On day 3 of culture protocol, 30 mL of cRPMI containing 20 ng/mL GM-CSF was added to each T175 flask. On day 6 flask supernatants were removed and replaced with 30 mL fresh cRPMI containing 20 ng/mL GM-CSF. On Day 7, 30 mL of cRPMI containing 20 ng/mL GM-CSF was added to each T175 flask. On day 10, loosely adherent cells were removed by gentle repeat pipetting. Cells were transferred to 50 mL falcon tube and centrifuged at 300 × g for 5 minutes at room temperature. The supernatant was discarded, and the cell pellet was resuspended in 10 mL cRPMI. Cell suspensions were adjusted to a final concentration of 6.25×10^5 cells/mL in cRPMI with 10 ng/mL GM-CSF. Cells were plated in round bottom 96 well plates at a volume of 200 μL/well. The plates were incubated for at least 2 hours at 37°C, 95% humidity and 5% CO2 before stimulation. Cells were treated with indicated inhibitors 40 minutes prior to stimulation with particles/controls. Control cells (“vehicle control”) were incubated with in the presence of corresponding amount of DMSO used in the inhibitor groups. Cells were then stimulated with particles/controls as indicated in the figures and were incubated overnight.

Culture and differentiation of mouse myoblast cell line C2C12 cells

Mouse myoblast C2C12 culturing protocol was based on the cell line product data sheet (ATCC). C2C12 cells were cultured at 37°C, 95% humidity and 5% CO_2 in T75/T175 flasks in cDMEM, and it is crucial to avoid cells becoming confluent over course of their subculture. To remove cells from flasks they were first washed with pre-warmed PBS, followed with trypsin-EDTA treatment for 5 minutes at 37°C. Cells were then harvested and centrifuged at 300 × g for 5 minutes at 37°C, and the cell pellet was resuspended in cDMEM for cell counting as described above. Cells were then plated in 24 well plates for cytotoxicity studies. C2C12 cells were plated at 5×10^3 cells per cm^2 of cell culture surface area. These cells were allowed to become confluent, usually after 3–4 days of culture and following confluency media was changed from standard cDMEM to cDMEM supplemented with 2% horse serum instead of 10% FBS, to encourage differentiation, usually occurring within another 3–4 days of culture. C2C12 cells undergo differentiation from myoblasts into myotubules, with indicative changes in morphology towards tightly packed, striated cells. Fully differentiated cells were then used for *in vitro* experimentation. 24 hours before stimulation cells were returned to cDMEM supplemented with 20% FBS. Particles were then added at concentrations indicated in the figures and plates were centrifuged at 200 × g for 3 minutes before cells were returned to the incubator.

METHOD DETAILS

Particle washing

Ultrapure, endotoxin-free, negatively charged polystyrene particles were purchased from Phosporex Inc (USA). Particles were vortexed for 2 minutes and washed using 2 cycles of centrifugation/suspension in 20 volumes of apyrogenic PBS to remove surfactants or stabilizers. Centrifugation velocity was determined as per Stokes’ Law according to particle size. Particles were suspended

at the appropriate concentration calculated as mg polymer/mL, mixed with the antigen and kept at room temperature for 40min before injection.

PLGA particle synthesis

To make 50–60nm particles, PLGA 50:50 (Sigma-Aldrich) and brain phosphatidylserine (PhS) (Lipoid) were suspended at a final concentration of 0.5 mg/mL (1:1 w/w) in DMSO (Sigma-Aldrich). Nanoparticles were produced using the NanoAssemblr® (Precision NanoSystems, Inc) at a flow rate ratio (DMSO/Tris buffer) 1:1 and a total flow rate 10 mL/min. Excess solvent removal and concentration of the particles to 20 mg/mL was achieved using the Krosflo Research IIi tangential flow filtration system (Spectrum Labs) with a 500 kD mPES column and a 12 mL diafiltrate volume. Particle size, polydispersity index and zeta potential was measured using a Zetasizer Nano ZS (Malvern Instruments, UK) equipped with a 633 nm laser and a detection angle of 173°. All measurements were undertaken in triplicate with the attenuation value between 6 and 9.

Antigen production

Apyrogenic ovalbumin (OVA) was from Hyglos GmbH (Germany). Influenza nucleoprotein peptide NP311-325 was from JPT Peptide Technologies (Germany). OVA-NP311-325 was generated by conjugation of Cys-NP311-325 to maleimide-activated OVA (ThermoFisher) as per manufacturer instructions. Recombinant *S. aureus* clumping factor A (ClfA) was produced and purified using DetoxiGel; endotoxin levels were <0.005 EU/mL by limulus amebocyte lysate (LAL) chromogenic endotoxin quantitation kit.

Mice immunisations

Intramuscular vaccination was done on days 0 and 14 using 27G/0.5in tuberculin needle in both hind limbs (biceps femoris muscles) using 50μL/leg. Animals received 10μg OVA alone or in combination with 1mg of particles (or alum/CpG/cGAMP) or PBS alone. For studies investigating the role of GSDMD, mice received the GSDMD inhibitor necrosulfonamide (NSA) i.p. (1.25mg) 1h before vaccination or i.m. (0.25mg) at the time of vaccination. For studies investigating the role of ROS, mice were treated with the ROS scavenger TEMPOL administered i.m. (25 mg/kg) or i.p (100 mg/kg). Subcutaneous immunization was done in the flanks on days 0 and 14, with a total volume of 100μL/mouse and previously determined optimal amounts of particles (4mg) and ClfA (1μg). For intraperitoneal vaccination the same immunization scheme was used. Mice received PBS alone, 1μg OVA alone or with 4mg of particles or 1mg alum in 200μL.

B16F-OVA melanoma challenge & CD8α T cell depletion

Mice were vaccinated i.m as before. Two weeks after booster vaccination, 3 × 105 B16F-OVA cells in exponential growth phase were implanted subcutaneously in a volume of 100μL. Mice were monitored daily; once the tumours became palpable the diameter of the lesion was measured using a callipers and tumour volume in mm3 was recorded. Animals were humanely euthanised when the lesion reached 1500mm3 or if necrosis was noted. For the CD8α+ T cell depletion, mice were injected i.p with 250μg of either a monoclonal α-CD8α antibody (Clone2.43) or a monoclonal isotype control antibody (Clone LTF-2) on day 26. Mice subsequently received injections of 100μg of the respective monoclonal antibodies on days 29, 33, 37, 41 and48. Blood was sampled from mice via the tail vein on days 31 and 35 to detect the presence of peripheral CD8+T cells. B16-OVA tumour cells were implanted on day 28.

Quantification and characterization of ag-specific T cells

Seven days after booster single-cell suspensions were prepared by mechanical dissociation of spleens using a 40μm mesh. After lysis with ammonium chloride buffer, 2 × 107 viable cells were suspended in 200μL of complete RPMI. Cells were stained with PE-labelled H-2K(b) Chicken OVA257-264 SIINFEKL or APC-labelled H-2K(b) I-A(b) NP311-325 QVYSLIRPNENPAHK from MBL or provided by the National Institutes of Health Tetramer Core Facility (Emory University) at 15 μg/mL for 2 h at 37°C in a tissue culture incubator (95% humidity and 5% CO2), with orbital shaking (200rpm). Anti-CD16/CD32 mAbs (1μL/sample) (BD) was added prior labelling with fluorescent antibodies for mouse F4/80 (Cl:A3-1) and CD8 (KT15) (Biorad), CD4 (GK1.5, eBiosciences), CD3 (17A2) and CD11c (N418) (Biolegend), CD44 (IM7) and B220 (RA3-6B2) (BD) and incubated for 20 min. After washing in PBS live-dead Aqua staining (BD) was added (1/500 dilution) for 30 min. After washing cells were suspended in 2%v/v buffered paraformaldehyde for 20 min, washed in PBS and suspended in 200μL of PBS+2%v/v fetal bovine serum and kept at 4°C in the dark until acquisition in a 4 laser/16 fluorescent parameter LSR-Fortessa analyzer at a maximum flow rate of 16,000 events/sec until reaching 1 × 106 live cells or 1.5 × 103 Tmer + cells. Analysis was carried out in FowJo (V10X, BD).

Quantification of cytokines

Seven days after booster, 4 × 105 splenocytes obtained as before were plated in triplicate in sterile 96 well U-bottom plates (200 μL/well) in the presence of absence of 20μg or 200μg of OVA, or plate-bound anti-CD3 (0.2 μg/mL). Cells were incubated at 37°C with 5% CO2 for 72h. Cytokines were quantified in cell-free supernatants using mouse IFN-γ DuoSet ELISA kits from R&D or ELISAMAX mouse IL-10 or IL-17A kits from BioLegend as per manufacturer's instructions.

Quantification ag-specific antibodies

Whole blood was collected on day 21. Clotting was allowed overnight at 4°C and serum was recovered after centrifugation for 10 min at 8000 xg. Samples were serially diluted 1:1 in assay diluent and incubated on antigen-medium-binding pre-coated plates (10 μg/mL OVA or 50 μg/mL ClfA in sodium carbonate buffer, pH 9.5). Ag-specific serum Ab titers were measured using a standard ELISA protocol and the following antibodies: goat anti-mouse total IgG-HRP from Southern Biotech (1/5000 dilution), biotin rat anti-mouse IgG1 from BD (1/4000 dilution), biotin rat anti-mouse IgG2b from BD (1/4000 dilution), and goat anti-mouse IgG2c-HRP from AbD Serotec (1/2000 dilution) and developed using streptavidin-HRP or OPD substrate directly as required. OD values were obtained using a VersaMax microplate reader at 492nm. Antibody concentrations were expressed as Log10 endpoint titers calculated by regression of a curve of OD values versus reciprocal serum levels to a cutoff point of 4 SD above the blank.

Magnetic sorting of $CD8^+$ T cells

$CD8^+$ T cells were magnetically sorted through negative selection from the spleen of vaccinated mice using a $CD8\alpha^+$ T cell isolation kit from Miltenyi Biotec according to the manufacturer's instructions. Magnetically sorted T cells were then stained according to the instructions above to identify antigen-specific $CD8^+$ cells.

Serum antibody neutralisation assay

The presence of neutralising antibodies in the serum was determined by testing the ability of serum from immunised mice to inhibit the adherence of *S. aureus* to fibrinogen. Microtitre plates were coated with fibrinogen (2μg/mL) overnight at 4°C and were subsequently blocked for 2 h at 37°C with 5% BSA. *S. aureus* PS80 cultures were grown to stationary phase, and were incubated with mouse serum (1:60 dilution) for 30 min at room temperature before being added to the wells of a fibrinogen-coated plate and incubated for 1.5 h at 37°C. After washing with PBS, adherent cells were fixed with formaldehyde (25% v/v), stained with crystal violet and the A570 measured. Adherence was expressed as a percentage of bacterial adherence in the absence of serum and percentage inhibition was determined by subtracting the percentage adherence values from 100.

Quantification of cell death

To quantify cell death, LDH assays were carried out according to the manufacturer's instructions. Firstly, a set of triplicates wells were lysed using addition if 10X lysis buffer and incubation for 45 minutes at 37°C, 95% humidity and 5% CO_2. 600μL of supplied assay buffer was added to 11.4mL of supplied substrate stock solution and was mixed to make up the reaction mixture and kept in the dark. Alternatively pre-made-up reaction was thawed. Assay was conducted to fresh cell supernatants to ensure greater accuracy. 50μL of supernatants were added to a 96 well flat-bottom plate in triplicate samples. 50μL of reaction mixture was added to each well and the plate was incubated for 30 minutes in the dark at room temperature. Following incubation, 50μL of supplied stop solution was added to each well, and the optical density (OD) values were determined by measurement of absorbance at 492nm using a plate reading spectrophotometer. Additionally, the absorbance was read at 680nm to account for any background absorbance values. This is especially apparent with larger PS nanoparticles (>100nm). Similarly, the vehicle control of added stimulants was added to a control set of triplicates to account for spontaneous LDH activity. % Cytotoxicity was calculated as follows for each absorbance:

$$\%\text{Cytotoxicity} = (\text{Compound} - \text{treated LDH activity} - \text{Spontaneous LDH activity}/ 100\%\ \text{lyse control LDH activity} - 100\%\ \text{lyse control LDH activity}) \times 100$$

Then the values obtained for cytotoxicity determined from the 680nm wavelength were subtracted from this obtained from those measured at the 492nm wavelength to account for background.

Immunoblotting

Murine BM-DCs were plated in 6-well plates, 2 × 106 cells/well and allowed to adhere. BM-DCs were either left unprimed or primed for 1 h with 10 ng/mL LPS. Following this priming step, cells were stimulated with either media, LPS alone (10 ng/mL), 50 nm PS (1 mg/mL) + LPS (10 ng/mL), or 1 μm PS (1 mg/mL) + LPS (10 ng/mL) for 18 h. Cells primed with LPS (10 ng/mL) and treated with nigericin (10μM) were used as a positive control. Following stimulation, cells were lysed using Laemmli sample buffer. Samples were then boiled with subsequent SDS-PAGE and immunoblotting. PVDF membranes were probed for full length and cleaved GSDMD protein (G7422, Sigma) and for β-actin (A5316, Sigma).

Cellular ROS quantification

Murine BM-DCs were plated in 12 well plates, 1.5 × 106 cells/well and allowed to adhere. Cells were stimulated with 50nm, 200nm or 1um PS particles at 3.9, 15.6 and 62.5 mg/mL for 6 or 18 h. Unstimulated cells were used as a control. Cells were then treated with 5μM of CellROX® Green reagent for 30 minutes at 37°C. After centrifugation at 1200rpm for 5 min, cells were recovered and stained with BV510 fixable viability stain for 30 min at 4°C. After washing in PBS and resuspension in FACS buffer samples were acquired in a BD FACS CANTO II and analysed in FlowJo software.

Endotoxin quantification

Endotoxin levels were quantified using a Pierce Chromogenic endotoxin quantification kit as per manufacturer's instructions.

QUANTIFICATION AND STATISTICAL ANALYSIS

Sample size was determined by power analysis based on existing data from pilot studies, where necessary experiments were carried in blocks to achieve the appropriate sample size. One-way ANOVA test was used to determine significant differences between multiple groups. Pairwise comparison of the means was done with the following post-hoc tests: Tukey's test (or Tukey-Kramer for unequal sample sizes) comparison between all groups; Dunnett's for multiple comparison between treatment groups and a pre-selected control group (typically antigen alone); Fisher LSD for pairwise comparisons of selected groups. Variance of the data was tested prior multiple comparison using Levene's test. If the homogeneity of variance was not met, data were transformed to Log10 values prior statistical analysis. Statistical significance for survival analyses determined by Mantel-Cox test. Statistical significance was set at $p \leq 0.05$. p values were represented as ****$p \leq 0.0001$, ***$p \leq 0.001$, **$p \leq 0.01$, *$p \leq 0.05$; ns $p > 0.05$. In some cases, the symbol "•" was used instead of asterisks to discriminate comparisons between treatment groups or against control.